ANL-6807

Argonne National Laboratory

HEAT AND MASS TRANSFER TO A GAS-FLUIDIZED BED OF SOLID PARTICLES

by

Edward N. Ziegler

Price $1.75 . *Available from the Office of Technical Services, Department of Commerce, Washington 25, D.C.*

ANL-6807
Engineering and Equipment
(TID-4500, 32nd Ed.)
AEC Research and
Development Report

ARGONNE NATIONAL LABORATORY
9700 South Cass Avenue
Argonne, Illinois 60440

HEAT AND MASS TRANSFER TO A GAS-FLUIDIZED BED OF SOLID PARTICLES

by

Edward N. Ziegler
Chemical Engineering Division

December 1963

Operated by The University of Chicago
under
Contract W-31-109-eng-38
with the
U. S. Atomic Energy Commission

TABLE OF CONTENTS

TABLE OF CONTENTS

LIST OF FIGURES

HEAT AND MASS TRANSFER TO A GAS-FLUIDIZED BED OF SOLID PARTICLES

by

Edward N. Ziegler

SUMMARY

The mechanism of heat and mass transfer from an exchange surface to a fluidized bed of solid particles has been studied. The work is subdivided into three interrelated parts.

In Part A, simultaneous heat and mass transfer experiments from the surface of a sphere are described for comparable situations in a gas stream and a gas-fluidized bed of solid particles. The systems were chosen so that the fluidized particles would have capacity for heat transport but not mass transport. It was found that solid particles in the fluidized state increased heat transfer 10- to 20-fold, whereas mass transfer was increased only 1 $\frac{1}{2}$ to 2 times. On the basis of the unique property of the particles for heat transport, and assuming analogous heat and mass transfer in the gas phase, it was concluded that in any mechanism of heat transfer in the fluidized state, 80 to 95 percent of the transfer must be accounted for by particle transfer. The remainder may be accounted for in a path solely in the gaseous phase.

In Part B the results of measurements of heat transfer coefficients from a porous sphere and a cylindrical heater to a bed of solids fluidized in an air stream are presented. The solid particles varied only in their thermal properties. The heat transfer coefficient was found to increase with heat capacity of the solid and was independent of the thermal conductivity of the solid. A model which predicts the observed relation of heat transfer coefficient to the thermal properties of the solid was utilized. This model is based on particle heat absorption and utilizes a statistical distribution of particle residence times. Particle residence times back-calculated from the model agree with residence times observed experimentally and calculated from simple theoretical models. A maximum Nusselt number of 7.2 is predicted for any fluidized system satisfying the assumptions of the model.

In Part C the mass transfer data for diffusion from an internal surface to a fluidized bed obtained in the first two parts are analyzed. A correlation based on dimensional analysis accurately predicts Sherwood numbers for transfer from a stationary sphere to a fluidized bed of nonadsorbing particles. A model is proposed to describe the more general case of a bed

of adsorbing particles. The model is found to agree with published data in those cases in which adsorption rates are highest. Discrepancies at lower adsorption rates are accounted for.

PART A

SIMULTANEOUS HEAT AND MASS TRANSFER TO A FLUIDIZED BED (HEAT TRANSFER MECHANSIM)

I. Nomenclature - Part A

C_p	Heat capacity of gas, Btu/lb-°F
D_p	Diameter of sphere, ft
D_{pf}	Diameter of fluidized particles, in.
D_v	Gas diffusivity, ft^2/hr
e	Bed void fraction, dimensionless
G	Superficial gas velocity, $lb/hr-ft^2$
G_e	Average gas velocity based on void area of bed, $lb/hr-ft^2$
h_r	Radiation heat transfer coefficient, $Btu/hr-ft^2-°F$
h_t	Total heat transfer coefficient, $Btu/hr-ft^2-°F$
h_c	$h_t - h_r$ = Experimental heat transfer coefficient of mechanisms other than radiation, $Btu/hr-ft^2-°F$
h'_c	Heat transfer coefficient for film convection in absence of fluidized particles, evaluated at G_e of fluidized bed, $Btu/hr-ft^2-°F$
k_g	Mass transfer coefficient, lb-moles/$hr-ft^2$-atm
k_y	Experimental mass transfer coefficient, $k_g P_a M_a$, $lb/hr-ft^2$
k'_y	Mass transfer coefficient in absence of fluidized particles, evaluated from Equation 5 at G_e of fluidized bed, $lb/hr-ft^2$
M_a	Molecular weight of air, lb/lb-mole
Nu	$(h_c D_p/\alpha)$
Nu'	$(k_y D_p/\rho D_v)$
P_a	Average partial pressure of air, atm
p_s	Saturation partial pressure of water vapor, vapor pressure corresponding to t_s, atm
p_g	Partial pressure of water vapor in the air, atm

$(p_s - p_g)_m$	Logarithmic-mean partial pressure difference, atm
Pr	$C_p\mu/\alpha$
q, q_p, q_f	Rate of heat transfer at interface, by particle transport, via gas film, Btu/hr-ft^2
Re	(GD_p/μ) Reynold's Number based on superficial gas mass velocity
Sc	$\mu/\rho D_v$
t_g, t_s	Bulk gas temperature, temperatures at surface of sphere, °F
$(t_g - t_s)_m$	Logarithmic-mean temperature difference, °F
W	Mass transfer rate, lb-moles/hr-ft^2

Greek

α	Gas thermal conductivity, Btu/hr-ft-°F
μ	Gas viscosity, lb/hr-ft
ρ	Gas density, lb/ft^3
λ	Latent heat of vaporization of water, Btu/lb-mole

II. Introduction

The phenomenon of heat transport in fluidized beds has been the subject of numerous studies in recent years. Of particular interest is the heat transfer between the bed and an internal or external surface. The results of work on this topic have been summarized extensively by Zenz and Othmer.[26] A review by Botterill[1] includes all but the most recent literature.

Several of the early investigators verified the improvement in heat transfer obtained with fluidized beds and offered accompanying rationales in the form of mechanisms of transport. For instance, Leva et al.[8-10] and Dow and Jakob[3] suggested that the increase in heat transfer was probably a consequence of the scrubbing action of particles against the transfer surface. This action was thought to disturb the gas film and hence decrease its resistance to the flow of heat. In later presentations, such as those of van Heerden et al.[18,19] Wicke and Hedden,[25] Wicke and Fetting,[24] Mickley and Fairbanks[11,12] and Ernst,[4] mechanisms were developed that appear to be more credible in explaining heat transfer improvement of the magnitude experienced.

Although there are some differences in these suggested models, common factors may be summarized as follows. The fluidized particles are visualized as a packet (i.e., a closely locked assemblage of particles) moving

from the core of the bed to the particular boundary surface, absorbing or giving up heat, depending upon the relative temperature of the surface, and then returning to the core of the bed. The interstitial gas serves as a stirring agent and as a heat transfer medium between the particles and the surface. In a recent article by Botterill et al.,[1a] it was shown that a single particle residing at a transfer surface absorbs a large quantity of heat in a short time by virtue of its relatively large volumetric heat capacity.

The presence of the particles most probably improves heat transfer by a combination of the two aforementioned effects (i.e., conveyance of heat from the packet to the surface on contact, and disturbance of the gas film adjacent to the surface). The simultaneous occurrence of these two effects has not as yet been demonstrated by experiment. It was the intention of this experimental investigation to verify the presence of these two effects and to determine their relative importance.

The experiments performed involve simultaneous heat and mass transfer from a solid object to a fluidized bed. The system was chosen to allow both the particles and the gas to take part in the transport of heat at the solid surface. On the other hand, the particles in this system were chosen so as to have negligible adsorbtivity for the diffusing species (measurements show low BET surface area) and consequently so as to have no capacity for mass transport. Therefore, the only mechanism of importance in mass transfer is the diffusion of mass through the surface gas film. In systems without fluidized particles at constant surface temperature and composition, it is known that the mechanisms of heat and mass transfer from a surface are analogous for low mass transfer rates. Both types of transfer may be considered to take place through a gas film near the solid surface. As a consequence of the analogous mechanisms for these conditions, the ratio of heat to mass transfer coefficients remains approximately constant, and there exists an equality of "j" factors[2] for both cases.

Upon the addition of fluidized particles to a system, it is known that the heat transfer coefficient can be improved significantly. The improvement of the mass transfer coefficient is studied herein and is used in the determination of a mechanism of heat transfer. For example, if heat is not tranferred via the particles, the mass transfer coefficient would no doubt increase by the same factor as the heat transfer coefficient. On the other hand, if the particles do have a part to play in heat transfer, a difference in the transfer factors for the two cases would be expected. The magnitude of this difference in transfer factors is then a measure of the amount of heat absorbed by the particles.

III. Experimental Techniques

The experimental equipment used is indicated in Figure 1. A 0.5-in.-diameter sphere was saturated with distilled water and then exposed to a metered stream of dry inlet air under various fluidized-bed conditions. The

sphere was formed from Johns-Manville Type VIII catalyst carrier, a clay-like material which after baking has been shown experimentally to have a convenient constant-rate drying period.[17] The solid sphere had a fine hole drilled through all but 1/32 in. of its thickness. A thermocouple was inserted in this hole and held there by the addition of more clay and rebaking. The error of measurement at 1/32 in. from the surface was approximated by means of a simple model (see Appendix A). The sphere was saturated with water and suspended from the thermocouple. As a consequence of the short height of suspension and the relatively low gas velocities, the sphere remained stationary. Temperatures were recorded throughout each run. The inlet and outlet air humidities were recorded by a General Electric dew point recorder[16] which had been calibrated to within 1°F. The reader is referred to Appendix A for a description of this apparatus. Temperatures of the air at inlet and outlet conditions were measured by thermocouples. When steady state had been achieved, the outlet humidity and sphere temperature remained constant until the falling rate period was reached. Copper, glass, and fused alumina particles were used as the fluidized medium. Their properties are given in Table 1.

Part A
Figure 1

EXPERIMENTAL APPARATUS FOR SIMULTANEOUS HEAT AND MASS TRANSFER FROM SPHERE TO AIR WITH AID OF FLUIDIZED PARTICLES

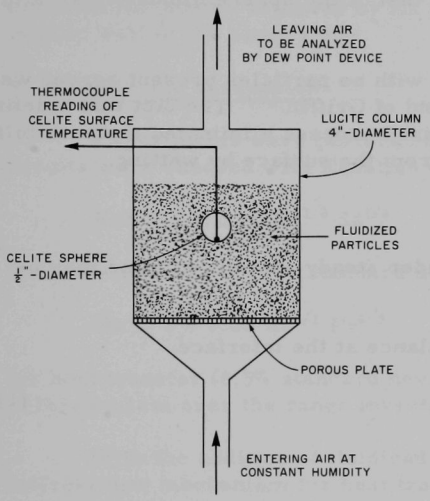

108-6707

Part A
Table 1

PROPERTIES OF FLUIDIZED SOLID PARTICLES USED IN EXPERIMENT

Fluidized Particles	Description	$D_{pf} \times 10^3$ (in.)	Density (lb/ft^3)	Heat Capacity (Btu/lb-°F)
Copper	Sharp	2.3	557	0.088
A-Fused Alumina	Sharp	5.8	243	0.183
B-Fused Alumina	Sharp	3.5	243	0.183
Glass	Round	4.5	154	0.188

The mass transfer coefficients were calculated from a knowledge of inlet and outlet dew points and the surface temperature of the sphere. The partial pressure of the water vapor in the nearly saturated air at the interface was assumed to be equal to the vapor pressure at the surface temperature. The heat transfer coefficients were calculated from a knowledge of the air temperature and surface temperature and the mass transfer rate as determined by dew point measurements. Allowance was made for radiant heat transfer. The transfer area was that of the sphere minus the area of the thermocouples.

The data for the single sphere with no particles present agreed well with those of Ranz and Marshall[14] and of Griffin.[7] The fact that a definite steady state was reached for the fluidized process eliminated the possibility of any appreciable removal of water from the surface by wetting.

IV. Analysis

The heat and mass transfer under steady-state conditions may be defined by the following equations:

For heat and mass transfer balance at the interface,

$$q = W\lambda. \tag{1}$$

For mass transfer rate,

$$W = k_g(p_s - p_g)_m = \frac{k_y}{P_a M_a}(p_s - p_g)_m. \tag{2}$$

For heat transfer rate

$$q = h_t(t_g - t_s)_m. \tag{3}$$

The quantities p_g and t_g vary little during the run. In addition, p_s is a function of t_s only. The coefficients k_g and h_t are independent variables, hence, depending on their values, a certain value of t_s, and thus of p_s, will be reached at steady state (i.e., the final value of the temperature at the surface is a function of only the heat and mass transfer coefficients when the dry bulb temperature and the partial pressure of the water vapor in the air have small variation). The coefficients k_g and h_t for most systems have been found to vary similarly, but they should not be thought of as mutually dependent. The transfer of heat and mass is interdependent, but the coefficients of heat and mass transfer are independent. Only under conditions at which heat and mass are transported by an analogous mechanism do k_g and h_t have similar variation.

For an air-water system, Ranz and Marshall[14] presented the following relation:

$$Nu' = 2 + 0.60\ Re^{1/2}\ Sc^{1/3}. \quad (4)$$

Equation 4 was developed from boundary layer theory as per Froessling[5] and from dimensional analysis. It is applicable for mass transfer in the Reynolds number range from 0 to 200. The analogous heat transfer equation with Nu' and Sc replaced by Nu and Pr, respectively, is found to hold equally well in the same range.

V. Results and Discussion

Experiments were performed without fluidized particles and the results were checked with Equation 4. The equations

$$Nu' = 2 + 0.56\ Re^{1/2}\ Sc^{1/3} \quad (5a)$$

for mass transfer (11.5% standard deviation of data), and

$$Nu = 2 + 0.68\ Re^{1/2}\ Pr^{1/3} \quad (5b)$$

for heat transfer (8.5% standard deviation), were used to represent the data of this system over the range investigated.

With the addition of fluidized particles to the system, however, an entirely new mechanism for heat transfer, particle transport (convenient name for transport via a path or paths which include particles), is available which has no equivalent in mass transfer for the conditions of the experiment. Therefore, for the system with fluidized particles, it is conceivable, and in fact, a reality, that the heat transfer coefficient can change significantly from that of the no-particle case with no comparable accompanying change in mass transfer coefficient.

Useful comparisons can be made from Table 2, which contains representative heat and mass transfer coefficients and their ratios for the

Part A
Table 2

REPRESENTATIVE EXPERIMENTAL DATA

Fluidized Particles	G(lb/hr-ft^2)	G/G_{mf}	h_c(Btu/hr-°F-ft^2)	k_y(lb/hr-ft^2-mole fraction)	h_c/k_y
None	145.6	-	3.12	12.3	0.253
	163.2		3.79	15.6	0.244
Copper Powder	70.0	3.18	34.0	21.4	1.59
	145.6	6.60	34.0	26.4	1.29
A-Fused Alumina	92.6	2.27	76.0	21.9	3.48
	145.6	3.57	73.3	24.5	2.99
B-Fused Alumina	92.5	5.78	62.4	23.7	2.63
Glass	72.3	3.61	100.9	23.9	4.22
	124.7	6.23	100.5	18.6	5.40

fluidized systems and empty tubes (complete data are given in Appendix A). For all systems of fluidized particles, a large increase in heat transfer coefficient occurs with a comparably minor increase in mass transfer coefficient. The ratio h_c/k_y is approximately constant (0.249, 4% standard deviation) for non-fluidized systems. This is in agreement with the "Lewis relation" (after W. K. Lewis) which states that h_c/k_y is approximately equal to C_s and is a consequence of the analogous mechanism of heat and mass transport. It has been shown that for the air-water system, the relation is applicable. For pure air, $C_s = 0.24$.

The ratio h_c/k_y is plotted in Figure 2 as a function of gas velocity over the entire experimental range. It may be noted that the variation in the ratio, thus represented, is slight. With fluidized particles present, however, the ratio varies considerably and is greater than 5.0 in some instances. It is apparent that the mechanism of heat transfer is not analogous to that for mass transfer in fluidized beds. Also, Equation 5 does not apply for systems with fluidized particles. The values of heat and mass transfer coefficient are plotted as a function of reduced gas velocity in Figure 3.

Part A
Figure 2

RATIO OF GAS-PHASE HEAT TO MASS TRANSFER COEFFICIENTS AS A FUNCTION OF AVERAGE GAS VELOCITY

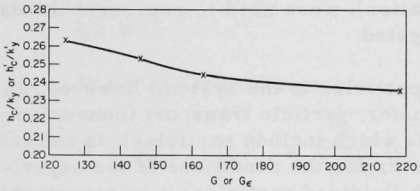

108-6257 Rev.

Mass Transfer Results

It is of interest to determine the effect, if any, of the moving particles on the gas-film mass transfer. In order to carry out a comparison of coefficients in systems before and after the addition of particles, it is essential that the comparison be made at identical average gas velocities so that any changes are not caused merely by a change in gas velocity. Therefore, the fluidized bed coefficient k_y is compared with k_y', defined as the coefficient before fluidized particles are added but at the same average gas velocity, G_e, as is present in the fluidized bed. The coefficient k_y' may be determined from Equation 5, which represents the "no particle" case for this experimental work, with G_e in the Reynold's number. In each case k_y is greater than k_y'. The factor of improvement, k_y/k_y' varies little in all systems studied, the highest value being about two. Representative values are shown for each of the systems in Table 3. Complete data are given in Appendix A.

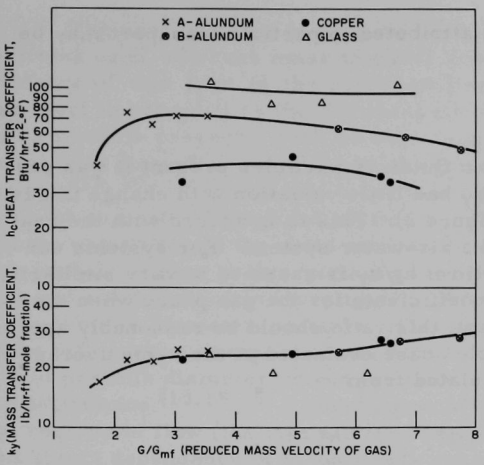

Part A
Figure 3

EXPERIMENTAL HEAT AND MASS TRANSFER COEFFICIENTS IN FLUIDIZED BED

108-6140 Rev.

Part A
Table 3

RELATIVE EFFECT OF PARTICLES ON FILM (REPRESENTATIVE VALUES)

Fluidized Particles	Void Fraction e	G_e, lb/hr-ft²	Btu/hr-ft²-°F h_c	Btu/hr-ft²-°F h'_c	Btu/hr-ft²-°F h_f	lb/hr-ft²-mole fraction k_y	lb/hr-ft²-mole fraction k'_y	$\frac{k_y}{k'_y} = \frac{h_f}{h'_c}$	$\frac{h_f - h'_c}{h_c} \times 100\%$
Copper	0.532	131.7	34.0	3.25	5.29	21.4	13.1	1.6	6.0
	0.632	172.2	42.3	3.62	5.76	23.0	14.5	1.6	5.0
A-Fused Alumina	0.784	159.0	73.3	3.51	6.15	24.7	14.1	1.8	3.6
	0.796	182.9	73.3	3.71	6.11	24.5	14.9	1.6	3.3
B-Fused Alumina	0.722	128.0	62.4	3.22	5.90	23.7	13.0	1.8	4.3
	0.751	144.6	57.9	3.37	5.30	27.0	13.5	2.0	5.8
Glass	0.570	126.9	100.9	3.22	5.92	23.9	13.0	1.8	2.7
	0.618	150.0	81.1	3.43	4.51	18.1	13.8	1.3	1.3

Heat Transfer Results

The heat transferred to the interface may be considered as

$$q = q_p + q_f, \tag{6}$$

where q_p is the heat transferred via particle transport and q_f is the heat transferred via the continuous gas phase. In terms of its heat transfer coefficient,

$$q_f = h_f(t_g - t_s)_m. \tag{7}$$

If radiation from the fluidized system surrounding the sphere is neglected, a reasonable assumption considering the temperatures of the experiments, h_t becomes equal to h_c. By combining Equations 3, 6, and 7, the fraction of

the total heat transport which is attributed to particle transport may be represented as

$$q_p/q = 1 - (h_f/h_c). \tag{8}$$

In the experiments with no fluidized particles present it was previously shown that the ratio h_c/k_y had little variation with change in gas velocity past the surface (see Figure 2). This is in accord with the heat and mass transfer analogy for the air-water system. For systems containing fluidized particles the ratio of h_f/k_y is assumed to vary similarly, since it represents the ratio of coefficients for the gas phase when the analogy continues to exist. In fact, this ratio should be reasonably approximated by h_c/k_y in the "no particle" case evaluated at the same average gas velocity. Hence, h_f may be calculated from

$$h_f = (h'_c/k'_y)\, k_y, \tag{9}$$

where h'_c/k'_y is obtained from Figure 2, by use of the average gas velocity G_e in the fluidized bed. It may be noted that interpolation between the discrete experimental values of gas velocity is necessary in using Figure 2, but it should be pointed out that an exact value of velocity is not necessary because very little change occurs in the ratio h'_c/k'_y. In fact, as mentioned earlier, the value of 0.249 may be used over the entire range of velocities with only 4% standard deviation.

If Equation 9, to compute h_f, and the experimental value of h_c are used, the ratio q_p/q may be calculated from Equation 8. Figure 4 is a plot of this ratio versus reduced mass velocity of the gas. This indicates eighty to ninety-five percent of the heat transfer, neglecting radiation, is by the particle-transport mechanism; the actual percentage depends on particle properties. If Equation 9 may be assumed to be correct, it is apparent that the factor of improvement of heat transfer in the gas film, h_f/h'_c, is exactly the same as the improvement factors for mass transfer, k_y/k'_y, listed in Table 2. Also included in Table 2 is the percent of the total heat transfer caused by the film disturbance, $(h_f - h'_c)/h_c \times 100\%$, for these systems. These values are less than 8 percent in all systems tested.

Part A
Figure 4

FRACTION OF HEAT ABSORBED BY PARTICLE

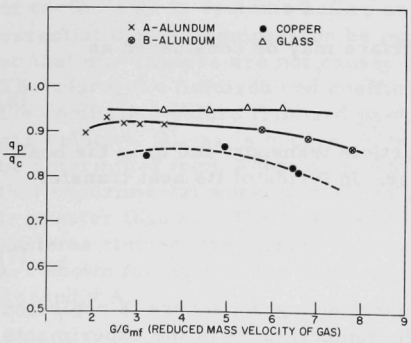

The heat transfer coefficient is dependent upon the kind of fluidized particles used, whereas mass transfer coefficients seem to have little dependence of this type in the range studied. If heat transfer by particle transport is accepted as the dominant mechanism, it is then understandable that a particle property, such as heat capacity, and a geometry factor, such as particle diameter, might be of considerable influence. In a number of articles[11, 19-23] it was concluded that h_c increases with increasing density and heat capacity of the solid particles. The exact relationship between h_c and the properties of the solid varied according to the different authors. The probable cause of this variation was the different conditions of gas flow rate and solid materials investigated. Likewise, an explicit dependency of h_c on particle diameter, valid for all conditions, could not be found because of the differences in experimental range and also as a consequence of the effect of particle diameter on bed porosity. In the work of Sarkits, Traber, and Mukhlenov,[13,15,16] a correlation of experimental data is divided into two regions of flow (the laminar flow regime and the turbulent flow regime). The direct dependency of h_c on solids density and heat capacity becomes weaker as the flow becomes more turbulent. Nevertheless, h_c increases with increasing values of these properties in both regions. The particle-diameter effect differs for the two regions, however. For laminar flow, h_c varies inversely with particle diameter, and for turbulent flow varies directly. Also, higher coefficients were obtained for smooth particles than for coarse particles. For a more detailed description of the conditions necessary for laminar and turbulent flow, the reader is referred to the original article.[16]

In the present investigation the smooth glass spheres of highest heat capacity gave the highest values of h_c and the sharper copper powder of lowest specific heat the lowest h_c values. Two sizes of fused alumina particles were used and gave little apparent variation in h_c. The values of h_c varied with the solid properties in a manner consistent with the previous articles cited. The depth of suspension of the sphere may be another variable of importance.

A diffusing species leaving the sphere disturbs the boundary layer of the gas and, therefore, produces some change in the overall heat transfer pattern. No exact quantitative measure of the effect of the radial velocity component of the diffusing species on heat transfer coefficient is available at the low Reynolds numbers of the experiment. At high Reynolds numbers, the data of Short, Brown, and Sage[16a] indicate that for 0.5-in. spheres, lower heat transfer coefficients exist for the case of systems undergoing simultaneous heat and mass transfer than for those with pure heat transfer. The difference between the two systems becomes smaller with decrease in Reynolds number. If the effect does occur to some extent at the low Reynolds number in fluidized beds, even more heat transfer would be accounted for by the absorption of heat by the particle. Correspondingly, the proportion of the heat transferred by the continuous gas phase will be less than was determined

herein. The effect of a velocity component perpendicular to the flow has, however, been shown to be negligible for flow over flat plates at low Reynolds number. It was, therefore, reasonable to assume that the error of omitting the effect of this component for flow around spheres at low Reynolds number would likewise be insignificant.

It might be stated in summary that for the region of gas velocities and particle properties studied, the predominant mechanism of heat transfer to a surface in a fluidized bed is that of particle transport. The other mechansim of additional disturbance of the gas film improved heat and mass transfer, but the heat transferred in this manner is only a small portion of the overall.

PART B

EFFECTS OF THERMAL PROPERTIES OF SOLIDS ON HEAT TRANSFER TO GAS-FLUIDIZED BEDS

I. Nomenclature - Part B

A_w	Surface area of heater, sq ft
C_s	Heat capacity of solids, Btu/(lb)(°F)
D_p	Particle diameter, ft
D_w	Characteristic wall dimension, ft
$f(\tau)$	Distribution function, dimensionless
g	Gravitational acceleration, ft/sec^2
G	Mass velocity of gas, lb/(hr)(sq ft)
G_{mf}	Mass velocity of gas at minimum fluidization point
h_c	Heat transfer coefficient at particle surface, Btu/(hr)(sq ft)-(°F)
h_o	Heat transfer coefficient at internal or external exchange surface
h_g	Heat transfer coefficient for surface to gas convection
k_g	Thermal conductivity of gas, Btu/(hr)(ft)(°F)
k_m	Thermal conductivity of quiescent bed
k_s	Thermal conductivity of solid particles
m	$18\ \mu/D_p^2\ \rho_s$, sec^{-1}
N	Particle Nusselt number, $h_c R_p/k_s$, dimensionless
Nu	Surface Nusselt number, $h_o D_p/k_g$
Pe	Peclet number, $C_s \rho_s D_p G/\rho_g k_g$, dimensionless
q	Heat flux from heater surface, Btu/(hr)(ft^2)
$Q(\tau)$	Instantaneous rate of heat absorption by particle at wall, Btu/hr
$\bar{Q}$	Mean value of Q, averaged over residence time
r	Radial position within sphere, ft
R_p	Particle radius, ft
s	$(\rho_s - \rho_g)g/\rho_s$, ft/sec^2
t	Temperature within sphere, °F
t_b	Temperature in bulk medium of the fluidized bed, °F
t_w	Temperature at internal or external surface, °F
T	Dimensionless temperature, $(t_w - t)/(t_w - t_b)$

Greek

α	Shape factor for gamma distribution
β	Scale factor for gamma distribution
μ	Gas viscosity, (lb)/(ft)(sec)
μ_p	Number of particles per unit area at heater surface, particles/ft^2
ρ_g	Gas density, lb/cu ft
ρ_m	Density of quiescent solid particles
ρ_s	Density of solid
θ	Particle residence time, hr
$\overline{\theta}$	Mean particle residence time, hr
τ	Dimensionless residence time, $k_s \theta / \rho_s C_s R_p^2$
$\overline{\tau}$	Mean dimensionless residence time

II. Introduction

Considerable quantitative information regarding heat transfer in fluidized-bed systems is available. However, no function of particle and gas properties, which suitably predicts the behavior of fluidized-bed heat transfer coefficients at internal and external heat-exchange surfaces, has been derived on theoretical grounds. In addition, the experimental data thus far available are not generally suitable for direct determination of the effects of properties of solids on the coefficients.

It is generally believed that the mechanism of heat transport between the particles and heat-exchange surfaces is one of heat absorption (or release) by the particle, with the gas serving as a heat transfer medium and as a stirring agent for the solids. This type of mechanism has been suggested by various investigators[23,27,15,9,4] and has been experimentally verified as discussed in Part A of this work. The particles leave the core of the bed, arrive at the surface, and absorb (or release) heat. The particles then return to the core of the bed.

Since the particles are presumed to be responsible for the rapid exchange of heat at the surface, it is of interest to determine the effect of their thermal properties on the heat transfer coefficient. Unfortunately, most solids of similar density have approximately the same heat capacity, and vice versa. Therefore, it is difficult to alter the heat capacity of the solids without a corresponding change in the density of the particles, and hence of their fluidization characteristics. This difficulty has been reported previously.[22] However, three materials of the same density, whose thermal properties vary over a reasonable range, have been found. These

are listed in Table 1, together with their pertinent properties. It may be seen that a tenfold variation in thermal conductivity and a twofold variation in heat capacity are obtained without significant variation in density. This fact permitted an investigation of the explicit effect of particle thermal properties on the heat transfer coefficient.

Part B
Table 1

PROPERTIES OF SOLID PARTICLES

Material	Density* (lb/cu ft)	Heat Capacity (at 77°F)* [Btu/(lb)(°F)]	Thermal Conductivity (at 77°F)* [Btu/(hr)(ft)(°F)]
Copper	559	0.092	223
Nickel	555	0.108	53
Solder (50% Pb, 50% Sn)	554	0.053	27

*Metals Handbook, American Society of Metals (1961).

Juxtaposed with the experimental investigation, a theoretical model has been developed which predicts the observed dependence of heat transfer coefficient on solid thermal properties, and agrees with previous data on the effect of gas conductivity.

III. Experimental Equipment

The experimental equipment used was similar to that described in Part A of this work. A complete description of the equipment and procedure will therefore not be given here, and only the essentials of the technique and the changes in the system will be noted. A 0.5-in. sphere of Celite is saturated with distilled and demineralized water. A constant supply of water to the sphere is maintained by a reservoir and siphon action, as shown in Figure 1. The vacuum system was employed to remove all air bubbles. The water passed through the smallest tube in the line, actually a 22 gauge hypodermic needle, before entering the sphere. Very fine thermocouple wires were passed through the hypodermic needle and were positioned 0.01 in. from the surface of the sphere. The error caused by the measurement being taken at a point this distance from the surface is small and less than the maximum calculated for a $\frac{1}{32}$-in. distance (see Appendix A). The sphere was submerged below the level of the stagnant bed. Temperature and humidity measurements were recorded for the gas at inlet and outlet conditions. The procedure for obtaining the heat and mass transfer coefficients was identical with the method described in Part A.

Part B
Figure 1

EXPERIMENTAL EQUIPMENT AND FLOW DIAGRAM

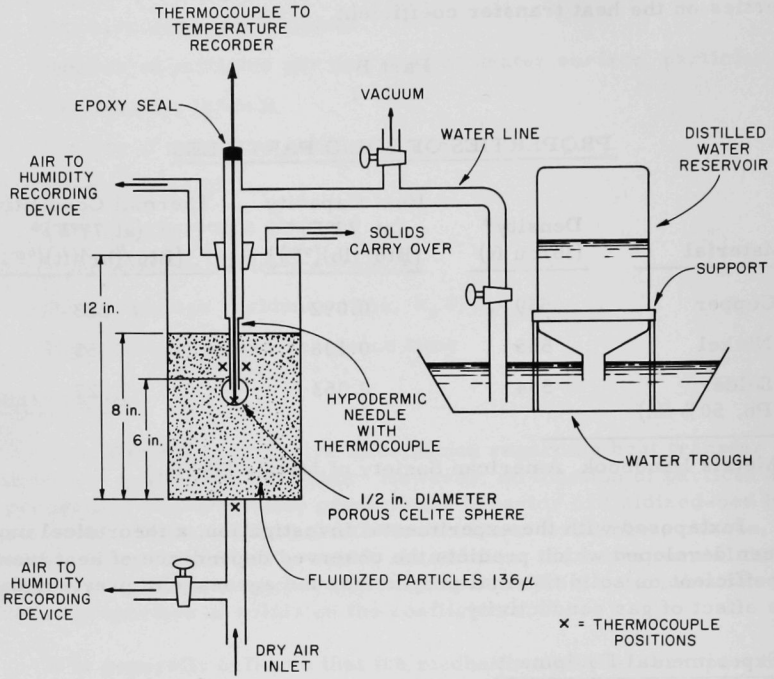

108-6496

In addition to the simultaneous heat and mass transfer experiment, pure heat transfer experiments were performed, with a cylindrical cartridge heater, 0.5 in. in diameter and 2.5 in. long. This heater, which was wound to give a uniform electrical heat flux over its surface area, was submerged in the bed to approximately the same position previously occupied by the Celite sphere. A thermocouple was soldered to the surface of the heater, and heat input was measured by a calibrated ammeter and voltmeter. Bed temperatures were measured at various positions and the average taken. For the fixed-bed cases, the logarithmic mean of the entering and leaving air temperatures was taken as the bulk temperature. The small sphere and heater were not expected to have significant variation in temperature along their surface when inside a dense phase fluidized bed. Therefore, the surface coefficients may be obtained from

$$h_o = q/A_w(t_w - t_b). \qquad (1)$$

The solid particles used were produced by an atomization process and were essentially spherical. The particles of half-and-half solder, nickel, and copper were carefully screened, and the 100 to 120 mesh (U.S. Standard Sieves) cut was chosen for the experimental work. The average particle size for this cut is 5.37×10^{-3} in. Photographs of these particles are presented in Figure 2. It can be seen that the particles were of essentially the same geometry and size, and hence differed significantly only in their thermal properties.

Part B
Figure 2
FLUIDIZED PARTICLES (Magnified 184X)

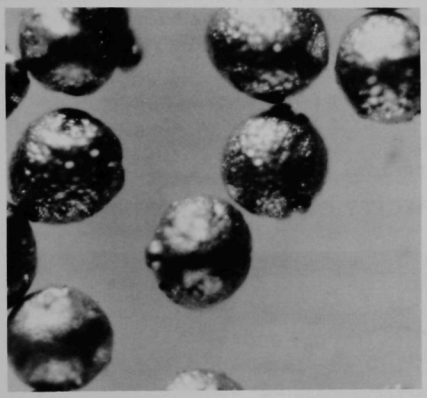

108-6600 2a
Copper

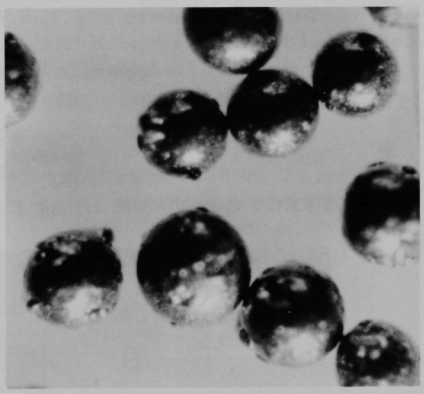

108-6599 2b
Solder

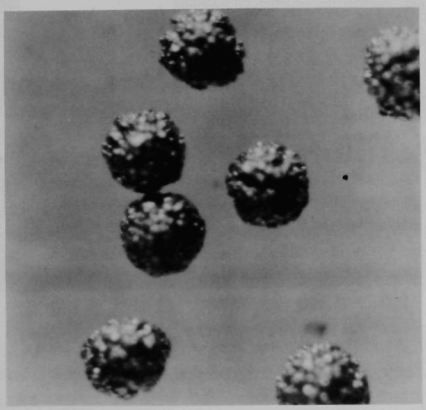

108-6598 2c
Nickel

IV. Experimental Results

The data obtained from the simultaneous heat and mass transfer experiments are given in Figure 3 as a plot of Nusselt number vs reduced mass velocity of the gas. Copper and nickel, materials of widely different thermal conductivities (see Table 1), produced a relatively small difference in Nusselt number. No systematic variation was determined for variation with solids thermal conductivity. On the other hand, the Nusselt number increased significantly with increased solids heat capacity. An increase of approximately fifty percent in the maximum Nusselt numbers occurred for a one hundred percent increase of heat capacity. The pure heat transfer experiments with a cylinder gave similar results, with somewhat higher Nusselt numbers at the same reduced gas velocities. In these, average Nusselt numbers of 6.1, 5.7, and 4.6 were obtained for the nickel, copper, and solder, respectively, in the fully fluidized beds. Complete data are presented in Appendix B for both pure and simultaneous transfer cases.

Part B

Figure 3

EFFECT OF SOLIDS HEAT CAPACITY ON NUSSELT NUMBER

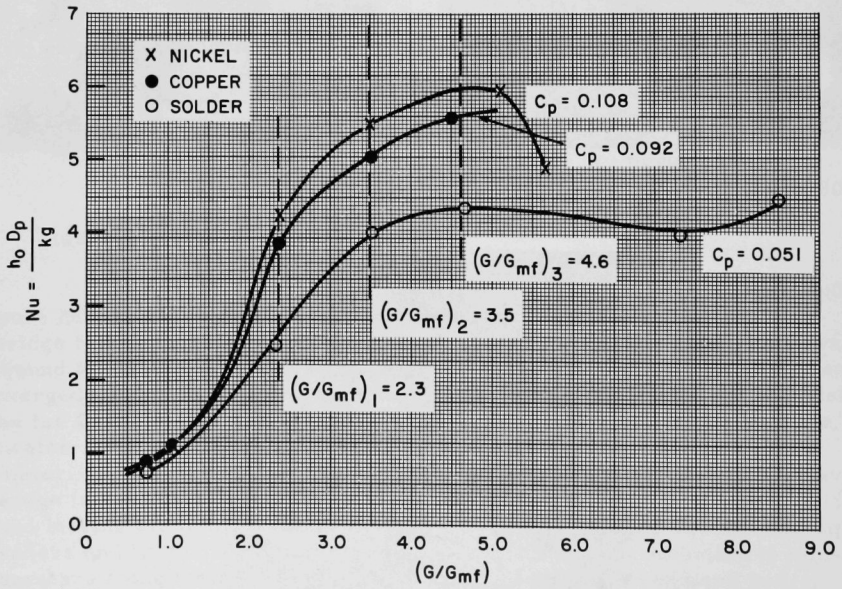

108-6503

V. Theory

In a recent publication,[28] a model for predicting heat transfer coefficients from surfaces to fluidized beds was developed based on the following assumptions:

"1. The fluidized particles are spheres of uniform diameter.

2. The physical and thermal properties of the solid and gas are constant.

3. Particles from the bulk of the fluidized medium arrive at the heating surface at the fluid bulk temperature, t_b. During the time that a particle remains at the surface it receives heat by convection from the fluid adjacent to the surface. This fluid is assumed to be at the surface temperature, t_w. After some time, the particle leaves the wall and returns to the bulk fluidized medium. This mechanism is pictured for a typical particle in Figure 4.

4. The major portion of the heat transfer occurs by the mechanism described in 3 above.

5. Radiant heat transfer from the surface to the particle is neglected. Baddour and Yoon[2] have shown this effect to be negligible in packed beds at temperatures below 600°C.

6. Conduction at the point of contact of the particles and surface is extremely small. Botterill et al.[4] have shown experimentally that this effect is negligible."

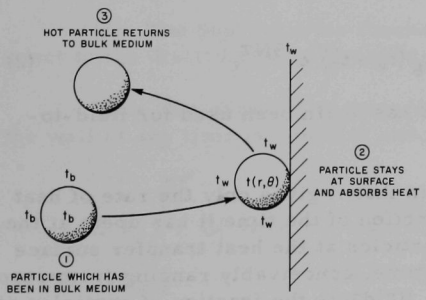

Part B
Figure 4

SCHEMATIC OF PROPOSED HEAT TRANSFER MECHANISM

108-6492

By applying the differential equation describing conduction in a sphere, the temperature profile within the sphere was derived. It was found[28] that by using the first term in the series solution (i.e., the first eigenvalue),

a solution representing the temperature at any point in the sphere with error less 2% was possible. This solution in terms of reduced quantities is

$$T = e^{-3N\tau} \tag{1}$$

when $N < 0.2$, where $N = (1/2)h_c D_p k_s$. It was reasoned that since the particle is near the wall, the surrounding fluid velocity will be small. Hence, the Nusselt number for fluid-to-particle convection, $h_c D_p/k_g$, was taken at its limiting value of 2 in the Froessling[10] expression. Then $N \approx k_g/k_s$. The requirement for Equation 1 to be valid to within 2% is, therefore, $k_g/k_s < 0.2$, as described.[28] The following material from the article co-authored with Koppel and Brazelton[28] is often referred to in the mass transfer analysis of Part C and is therefore, for purpose of comparison, quoted directly.

"Equation 1 may be derived on the basis of negligible thermal gradients within the particle. Thus, if the particle is at a uniform temperature $t(\theta)$, then

$$\rho_s C_s (\pi D_p^3/6) \frac{dt}{d\theta} = h_c \pi D_p^2 (t_w - t)$$

with

$$t(0) = t_b.$$

By introducing the appropriate dimensionless variables it is found that Equation 1 is once again the solution.

Equation 1 was used to calculate the rate of heat absorption by the particle from the formula

$$Q(\tau) = h_c 4\pi R_p^2 (t_w - t) = 4\pi R_p k_g (t_w - t_b) e^{-3N\tau}, \tag{2}$$

where the limiting Nusselt number of 2 has again been used for fluid-to-particle convection.

Equation 2 is limited in utility in that it gives only the rate of heat absorption of a single particle, as a function of the time it has spent at the surface. At any instant of time, the particles at the heat transfer surface have been there for various lengths of time, conceivably ranging from zero to infinity. Let $f(\tau)$ be defined so that $f(\tau)d\tau$ is the fraction of particles at the surface, at any instant, which have resided at the surface for a dimensionless time between τ and $\tau + d\tau$. Physically, one would expect some preferred range of residence times, so that $f(\tau)$ should go through a maximum. Using these qualitative ideas, it is convenient to select the gamma distribution function

$$f(\tau) = \frac{1}{\alpha!\,\beta^{\alpha+1}} \tau^{\alpha} e^{-\tau/\beta} \tag{3}$$

as descriptive of the distribution of dimensionless residence times for particles at the surface at any given instant. This distribution is pictured for various values of α at a single value of β in Figure 5. From Equation 3, the average residence time is determined as

Part B
Figure 5

EFFECT OF α ON GAMMA DISTRIBUTION

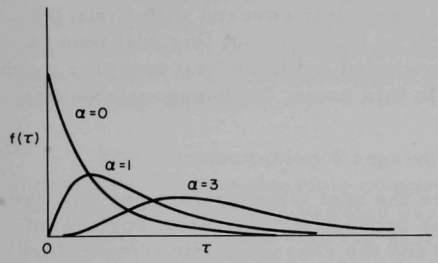

108-6495

$$\overline{\tau} = \int_0^\infty \tau f(\tau) d\tau = \beta(\alpha + 1), \qquad (4)$$

and the residence time of maximum probability (by differentiating Equation 3 and setting the result to zero) is

$$\tau_{max} = \beta\alpha. \qquad (5)$$

It can be seen from Figure 5 that α is merely a shape factor, determining the shape of the distribution. The smaller the value of α, the more sharply is the distribution peaked around its maximum. On the other hand, τ and τ_{max} are directly proportional to β, which therefore determines the location of the peak. Other distributions could undoubtedly be selected for the particle residence times, but the gamma distribution has the following advantages, besides being compatible with one's intuitive feeling for the shape of the true distribution:

(1) The shape of spread of the distribution may be altered considerably through the single parameter α.

(2) The heat transfer function $Q(\tau)$ is easily integrated with respect to the distribution of Equation 3.

Thus, the average or mean rate of heat absorption for particles at the wall at any time is constant and given by

$$\overline{Q} = \int_0^\infty Q(\tau) f(\tau) d\tau = \frac{4\pi R_p k_g (t_w - t_b)}{\left(1 + \frac{3N\overline{\tau}}{\alpha + 1}\right)^{\alpha+1}}. \qquad (6)$$

In order to obtain the heat transfer rate at the heating surface per unit area, it is necessary to estimate the surface concentration of particles, μ_p, in particles per unit area. From physical observations of fluidized systems it is noted that the column wall is, in general, almost completely coated with particles. Hence, if the fluidized bed is externally heated, for a first-order estimate of μ_p it can be assumed that the wall is

completely covered with particles in hexagonal packing. Even if the heater is internal, the fluid velocity at the heating surface is zero, just as in the external case. Since particles pack on the outer wall because of the required downward motion due to low fluid velocities, we may assume a similar behavior in the case of an internal surface. This is approximately confirmed by the data of Brusenback,[6] who measured particle concentrations at an internal surface in a fluidized bed and found them to be 80-100% of the corresponding values for the fixed bed in typical ranges of the operating variables. By assuming the surface to be completely covered with particles, the resulting particle concentration will be too high, but this will tend to compensate for the fact that we have excluded from the heat transfer mechanism all but the surface particles. On this basis, for hexagonal packing

$$\mu_p = 1/2R_p^2 \sqrt{3}. \tag{7}$$

The product of Q and μ_p gives the heat transfer rate per unit area, which may be equated to $h_o(t_w - t_b)$, the product of the overall surface-to-fluidized bed heat transfer coefficient and the characteristic temperature difference. Solution of this for the Nusselt number and reversion to the original variables yield the final result:

$$Nu = \frac{h_o D_p}{k_g} = \frac{4\pi/\sqrt{3}}{\left(1 + \dfrac{3k_g\bar{\theta}}{\rho_s C_s R_p^2(\alpha+1)}\right)^{\alpha+1}}. \tag{8}$$

Before examining the implications and accuracy of Equation 8, it is desirable to re-examine assumptions 3 and 4. Assumption 3 requires that the particles at the wall receive heat as if they were surrounded by a fluid medium at t_w. Actually, thermal gradients are realized in the surrounding fluid. Botterill[3] has solved numerically the unsteady conductive temperature field which results from a single glass sphere in plane contact with a wall that is 10°C hotter than the surrounding air medium. From this field, he calculated the instantaneous rate of heat absorption by the particle as a function of time. His results are replotted for a 200-μ glass sphere in Figure 6. In addition, the values of $Q(\theta)$ calculated from Equation 2 for the same conditions are plotted for comparison. It may be seen that good agreement is obtained in the vicinity of $\theta = 0.11$ sec, but the agreement elsewhere is poor. However

Part B
Figure 6

COMPARISON OF MECHANISM WITH THAT OF BOTTERILL AND WILLIAMS[3]

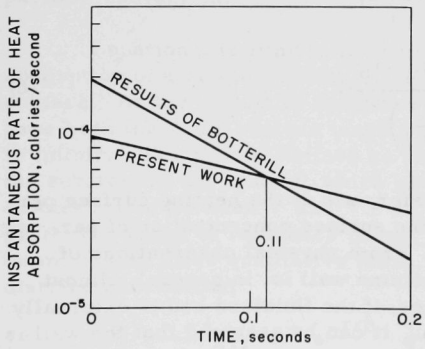

108-6494

0.11 sec will later be seen to approximate typical values of θ_{max} for fluidized systems. Thus, the integration process of Equation 6 tends to weight most heavily the more accurate values of $Q(\theta)$, and to average out the positive and negative deviations between the two curves of Figure 6. For this reason, it appears that the inaccuracies in assumption 3 are largely canceled by the statistical averaging process.

Although Botterill's results for 200-μ spheres justify assumption 3 for small particles, it is to be expected that for spheres considerably larger than 200 μ, the validity of this assumption will decrease. This is because larger particles are subjected to a greater variation in temperature of the surrounding medium.

To test assumption 4 regarding order of magnitude, it may be assumed that the only plausible competing mechanism for heat transfer is convection to a particle-agitated gas phase. If this mechanism is assumed to be acting in parallel with the particle pick-up mechanism, then another term $h_g(t_w - t_b)$ should be added to $\bar{Q}\mu_p$ in the equation with $h_o(t_w - t_b)$. In place of Equation 8, this would result in

$$\frac{h_o D_p}{k_g} = \frac{4\pi/\sqrt{3}}{\left[1 + \frac{3N\bar{\tau}}{\alpha + 1}\right]^{\alpha+1}} + \left(\frac{h_g D_w}{k_g}\right)\frac{D_p}{D_w}, \qquad (8a)$$

where D_w is a characteristic dimension of the heat transfer surface. For an externally heated bed, this would be the column diameter. The first term on the right side of Equation 8a is of the order of 1, and D_p/D_w is typically of the order of 10^{-3}. Under fluidized conditions, a typical Reynolds number based on column diameter would be 10^3, indicating a generally laminar type of flow. Therefore, even if particle agitation increased the gas convection by an order of magnitude [which is unlikely in view of the fact that Rowe and Partridge[20] have observed the fluid motion to be largely streamline], the Nusselt number for gas convection, $h_g D_w/k_g$, would not exceed 100. Hence, the second term on the right of Equation 8a can safely be neglected. Similar arguments can be offered to give the same conclusion for an internal heater."

VI. Agreement of Theory with Data

As a means of determining the validity of the model, various values of the shape factor α were chosen, and Equation 8 was rewritten in a form suitable for comparison with the data. For instance, for $\alpha = 0$ a plot of $1/h_o$ vs $1/C_s$ for constant values of G/G_{mf} should result in a straight line, as all other properties of the solid and gas are constant. Likewise, for $\alpha = 1.0$, plots of $1/\sqrt{h_o}$ vs $1/C_s$ should result in straight lines. Such a series of plots are given in Figure 7 for different values of α. The values

Part B
Figure 7

PLOTS FOR CALCULATING AVERAGE RESIDENCE TIMES AT VARIOUS VALUES OF α. a) $\alpha = 0$; b) $\alpha = 0.1$; c) $\alpha = 0.5$; d) $\alpha = 1.0$; AND e) $\alpha = \infty$

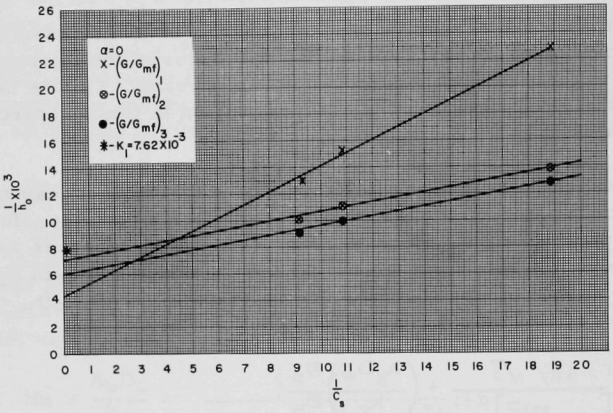

(a)

108-6497

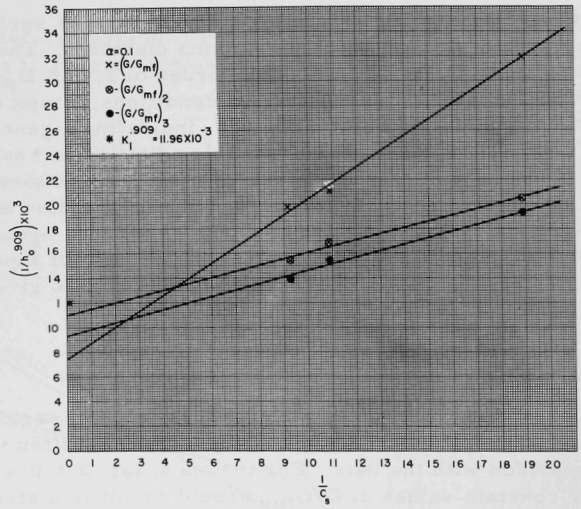

(b)

108-6498

Part B
Figure 7 (Contd.)

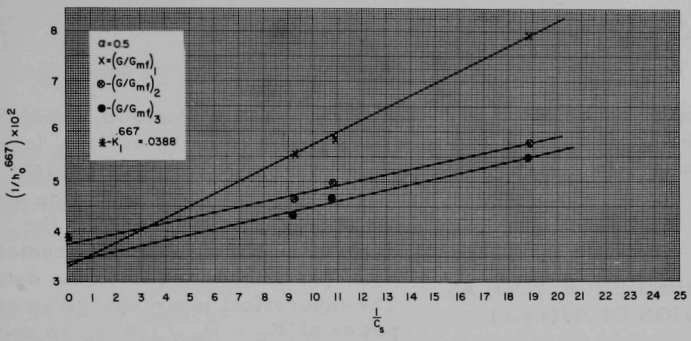

(c)

108-6502

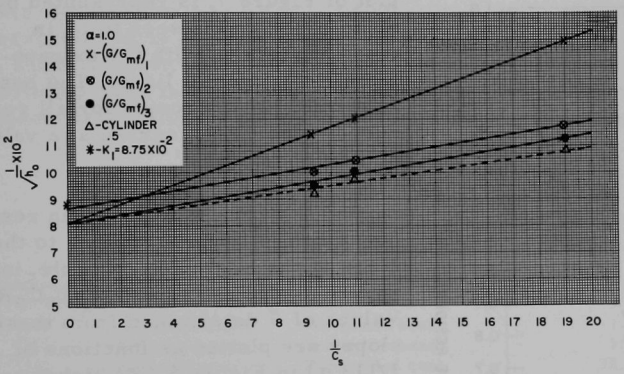

(d)

108-6501

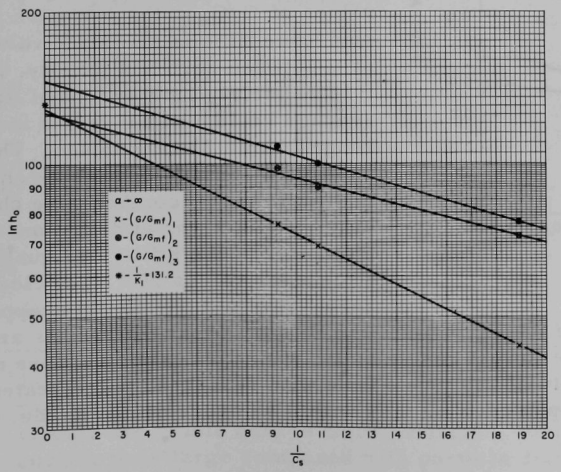

(e)

108-6499

of G/G_{mf} used are from Figure 3. As α approaches infinity, a special form of Equation 8 is obtained, namely,

$$Nu = \frac{4\pi}{\sqrt{3}} e^{-3k_g \bar{\theta}/\rho_s C_s R_p^2}. \qquad (9)$$

(This result may also be obtained by assuming every particle to reside for the average residence time $\bar{\theta}$.) In this case, a plot of ln h_o vs $1/C_s$ (see Figure 7e) should give a straight line. In all cases, reasonably straight lines result. A good indication of the accuracy of the model is the agreement of the intercept predicted with that determined from the data. The theoretical intercept, given as a power of $K_1 = D_p\sqrt{3}/4\pi k_g$ in each plot of Figure 7, is represented by an asterisk and is seen to be in close agreement with the extrapolated experimental lines. The best agreement of intercepts for all reduced velocities occurred at a value of α of about one.

Part B
Figure 8

AVERAGE RESIDENCE TIME AS A FUNCTION OF $1/(1+\alpha)$

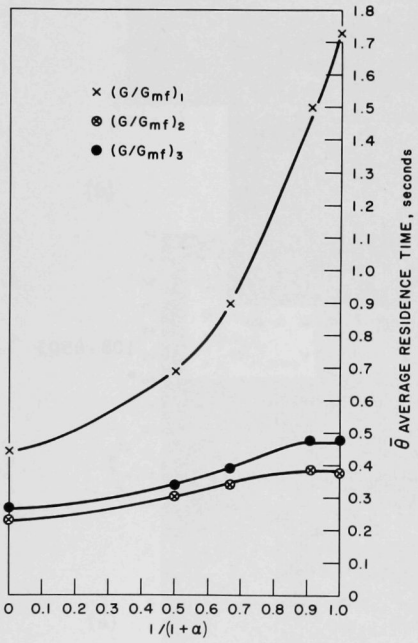

108-6493

In each case, the mean residence time $\bar{\theta}$ is proportional to the slope of the line. For example, in Figure 7c the slope is $3k_g\bar{\theta}/\rho_s C_s R_p^2$. Values of $\bar{\theta}$ determined from these slopes are plotted as functions of $1/(1+\alpha)$ in Figure 8. At higher values of G/G_{mf}, the variation in residence time is small for values of α between zero and infinity, and $\bar{\theta}$ is relatively independent of α; the average residence times are in the range from 0.23 to 0.45 sec. The relative insensitivity to large changes in α and, hence, considerable change in the shape of the distribution, is indicative of the utility of Equation 8. Except for values of α very close to zero (zero is a physically unappealing value for α because $\theta_{max} = 0$), it can be stated that the results are insensitive to α. At the lowest gas velocity, where all particles were not in motion, the sensitivity of residence time with respect to α is greatest. Even here the total $\bar{\theta}$ span over all α is within an order of magnitude.

A plot of the data for pure heat transfer from a cylinder is included in Figure 7d. The heat transfer coefficients used here were the average of values at three gas velocities in the high G/G_{mf} range. An average residence time $\bar{\theta}$ of 0.29 sec was determined for the cylinder.

VII. General Discussion of Model

It is interesting to observe the effect on the model of extreme conditions. Equation 8 predicts that the maximum observable value of the Nusselt number is $4\pi/\sqrt{3}$, or approximately 7.2. This situation will be approached for very short residence times (good mixing) or for very high volumetric heat capacity of the solid.

This conclusion, which can only be made under conditions for which the model is applicable,[1] gains some support from the heat transfer work of other experiments. In Table 2 a list of maximum observed Nusselt numbers, taken from a series of investigations available in the literature, is presented. It is significant that only one of all these experimental values is slightly above the predicted maximum, and all others fall below. The particles used in this work were fairly large and, as explained earlier, the model loses validity in the large particle range. In the correlation of

Part B
Table 2

MAXIMUM OBSERVED NUSSELT NUMBERS FOR FLUIDIZED BED HEAT TRANSFER

Reference	Transfer Surface	Solid Particles	D_p(ft) x 10^4	Max Nu = $h_o D_p/k_g$
(16)	Internal heater	Scotchlite beads	1.5	3.9
(16)	External wall	Scotchlite beads	1.5	2.3
(13)	External wall	Pulverized coal	38.6	4.5
(11)	External wall	Iron catalyst	3.6	1.7
(1)	Internal heater	Round sand	28.8	8.1
(26)	Internal cooler	Sharp Maas sand	11.6	2.6
(8)	External wall	Spheroidal catalyst	5.6	4.7
(24)	External wall	Carborundum	7.4	3.0
(25)	Internal cooler	Sharp silver sand	7.1	3.7
(19)	Internal heater	Ottawa sand (spheroidal)	3.9	3.0
(21)	External wall	Scotchlite beads	12.3	5.1
(27)	Internal heater	River sand (rough round)	1.0	4.6 (CO_2)
(12)	External wall	S/V Sovabead	129	5.8
(18)	Internal cooler	Alumina-nickel catalyst	11.5	5.0
(17)	Internal cooler	Silicon carbide	8.2	3.6 (CO_2)
(5)	Internal heater	Quartz sand	14.7	6.7
(14)	Internal heater	Scotchlite beads	10.5	5.6
(3)	Internal heater	Spherical lead glass	6.6	3.5
This work	Internal surface	Nickel spheres	8.4	6.2

[1] Jakob and Osberg[10a] measured Nusselt numbers as high as 11 for transfer from a submerged wire. However, the present model is obviously applicable only to transfer from a surface whose radius of curvature is large compared with particle diameters.

Vreedenberg,[25] transformed on Figure 9 to coordinates of Nusselt number vs Peclet number, a definite maximum Nu level is approached with increasing Peclet number. This level is visibly below the predicted maximum.

Part B
Figure 9

VARIATION OF NUSSELT NUMBER WITH PECLET NUMBER

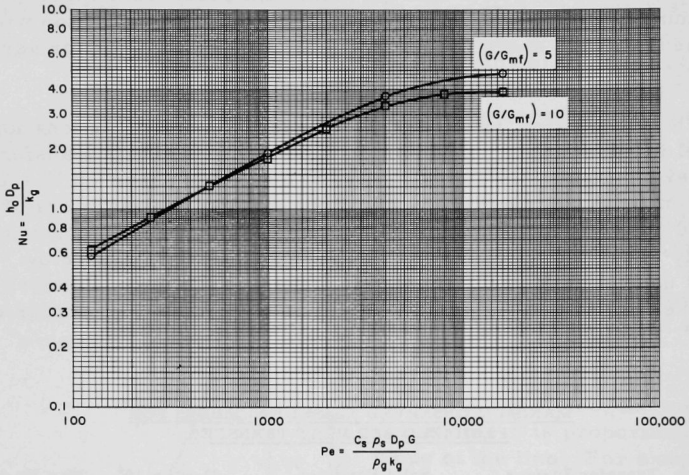

108-6500

The dependence of heat transfer coefficient on gas conductivity predicted by Equation 8 can be estimated for the experimental conditions of the present work, where the factor $3k_g \bar{\theta}/\rho_s C_s R_p^2$ typically assumed the value of 2/3. Then from Equation 8, for the typical value $\alpha = 1$,

$$\frac{h}{h^*} = \frac{(k_g/k_g^*)(16/9)}{[1 + (1/3)(k_g/k_g^*)]^2} \qquad (10)$$

where k_g^* is the base value for air, for which 2/3 is realized for $3k_g^* \bar{\theta}/\rho_s C_s R_p^2$, and h^* is the corresponding base heat transfer coefficient. For $k_g/k_g^* = 2$, Equation 10 predicts $h/h^* = 1.3$, and for $k_g/k_g^* = 1/2$, Equation 10 predicts $h/h^* = 0.65$. On logarithmic coordinates, these three values give a slope of 0.5, in reasonable agreement with the value of 0.6 suggested in the literature.[26a]

The model in its present form cannot be used to predict the effects on Nusselt number of R_p, ρ_s, and G, because these variables influence $\bar{\theta}$ (and probably α).

A model of heat transfer derived by Mickley and Fairbanks[15] has also separated the heat capacity effect from nonthermal properties. Their equation takes the form

$$h_o = \sqrt{\rho_m k_m C_s S}\,, \tag{11}$$

where

ρ_m = mean density of quiescent bed;

k_m = quiescent conductivity of particle packets;

S = stirring factor, a function of particle packed residence times.

Equation 8 has several advantages over this equation, both in utility and validity. First, the value of h_o in Equation 11 is directly proportional to the square root of C_s. This would imply that as C_s approaches infinity, h_o would likewise become infinite. As shown by experimental data, and as predicted by Equation 8, this is contrary to fact. Secondly, the value of h_o in Equation 11 depends on a stirring factor. This factor is a function of the residence time of particle packets, a value difficult to ascertain experimentally. Equation 8 is based on residence times of individual particles, an easier quantity to measure. Finally, the h_o value of Equation 11 is dependent upon the thermal conductivity of the bed of particles in their quiescent state. This would appear to indicate a dependence on both k_g and k_s. Upon analyzing the data of Mickley et al.,[14] it is found that the quiescent bed conductivity is almost exclusively dependent on gas thermal conductivity, and therefore the observed variation in h_o with k_m is probably due largely to variations in k_g, as predicted by the present model.

Residence Times

It is of interest to compare the residence times back-calculated from Equation 8 with those measured experimentally by other workers and with those from simple theoretical models. van Heerden et al.[23] observed particle residence times of one second at the external wall of a fluidized bed. Mickley et al.[14] observed residence times of 0.15-1 sec at an internal heater in fluidized beds under various conditions. Brusenback[6] observed bubbles at a heater surface with frequency of the order of 0.5 sec. This would represent the maximum residence time of his glass bead system.

As a simple model, consider the free fall of a spherical particle at the surface of an internal heater. For free fall with zero initial velocity,

$$\bar{\theta} = \sqrt{2(y - y_o)/g}\,,$$

where $y - y_o$ is the heater length and g is the acceleration of gravity. For a cylindrical heater which is 2.5 in. long, this free-fall equation predicts $\bar{\theta} = 0.11$ sec.

Instead of assuming free fall, we may assume the fluid to be viscous and that Stokes' law is applicable. Then

$$\frac{d^2y}{d\bar{\theta}^2} + m\frac{dy}{d\bar{\theta}} - s = 0, \tag{12}$$

where

$$m = 18\ \mu/\rho_s D_p^2, \text{ and } s = [1 - (\rho_g/\rho_s)]g.$$

Integration of Equation 12 gives

$$y - y_o = \frac{s}{m}\left(\bar{\theta} + \frac{1}{m}\ e^{-m\bar{\theta}} - \frac{1}{m}\right). \tag{13}$$

Substitution of a series expansion for $e^{-m\bar{\theta}}$ and retention only of terms up to second order results in the equation

$$y - y_o = \frac{s\bar{\theta}^2}{2}\left(1 - \frac{m\theta}{3}\right). \tag{14}$$

Using the properties of the fluidized system and a heater length of 2.5 in., as in the cylinder experiment, we obtain $\bar{\theta} = 0.12$ sec. Therefore, only a small change in $\bar{\theta}$ is found if the gas viscosity and density are taken into account. This might be anticipated because of the relatively low viscosity of gases at room temperatures and pressures, and the low densities of gases compared with those of solids.

These calculated average residence times are minimum values for particles falling with an initial vertical velocity component equal to zero. Particles falling along a contact surface of a fluidized bed are actually hindered by other particles adjacent to them. The true average residence time, therefore, is expected to be greater than that predicted from Equation 14. The average value calculated from Equation 8 for the cylindrical heater is 0.29 sec. No simple calculational analogue is available for estimating a lower bound on $\bar{\theta}$ in the case of a spherical surface.

VIII. Conclusions

1. The thermal conductivity of the solid, k_s, has negligible effect on the surface-to-fluidized bed heat transfer coefficient, h_o.

2. The coefficient h_o increases with increasing heat capacity of the solid, C_s. The rate of increase is less than linear.

3. A model based on absorption of heat by the particle, in which a statistical distribution of particle residence times is used, leads to

Equation 8, which predicts the experimentally observed dependence of h_o on C_s and k_s. Further, the derivation of Equation 8 predicts that h_o is independent of k_s only if $k_s/k_g > 5$.

4. Equation 8 predicts that the maximum attainable Nusselt number for transfer from internal or external surfaces to gas-fluidized beds is approximately 7.2. This conclusion, which is supported by data in the literature, is valuable for process optimization, as it provides a standard of excellence.

5. The model reduces the problem of determining the effects of thermal and physical properties on h_o to one of determining the effect of physical properties on particle residence times. The distribution function $f(\tau)$, which should not be overly difficult to measure on external surfaces, is a function of nonthermal properties only. A theoretical approach for determining the dependence of particle residence time on nonthermal properties is also feasible.

6. The predicted dependence of h_o on k_g in Equation 8 is in agreement with previous correlations.

7. Particle residence times back-calculated from heat transfer coefficients were in agreement with previous observations and with results of simple theoretical models.

PART C

MASS TRANSFER TO FLUIDIZED SOLID PARTICLES

I. Nomenclature - Part C

a	BET surface area, sq ft/lb
a_{ext}	external surface area of particle, surface of particle contacted by flowing gas stream, sq ft
a_p	total particle surface area, sq ft
C_{Tp}	mass capacity of solid adsorbent, lb/(lb/cu ft) (lb adsorbent)
D_a	diameter of a sphere having same external surface area as the actual particle, ft
D_p	average particle diameter, geometric mean of sieve sizes, ft
D_s	diameter of sphere having same volume as actual particle, ft
D_w	characteristic dimension of the exchange surface, ft
$D_\$$	characteristic dimension of spherical exchange surface, sphere diameter, ft
e	bed voidage or porosity, dimensionless
$f(t)$	distribution function for particle residence time, dimensionless
g	gravitational acceleration, ft^2/hr
G, G_{mf}	mass velocity of gas, velocity at minimum fluidization, lb/(hr)(sq ft)
G_e	G/e, lb/(hr)(sq ft)
k_c	mass transfer coefficient in still gas, ft/hr
k_w, k_g	overall mass transfer coefficient, gas-phase coefficient, ft/hr
m	mass flow of diffusing species, lb/(hr)(sq ft)
r	radial distance, ft
R_p	radius of particle (average), ft
R_s	radius of sphere having same volume as actual particle, ft
Re	GD_p/μ, dimensionless
Re_e	$GD_p/\mu e$, dimensionless
Sc	μ/pD_v, dimensionless
Sh	$k_g D_w/D_v$, dimensionless
Sh_e	value tabulated in Table 1 as a function of Re_e and Sc, dimensionless

Sh'	(D_p/D_w) Sh, dimensionless
Sh'_w	$k_w D_p/D_v$, dimensionless
t	particle residence time, hr
$\bar{t}$	average particle residence time, hr
v_p	particle volume, cu ft
x	particle concentration, lb adsorbed/lb adsorbent
x_b, x_v	bulk particle concentration, concentration while in laminar layer, lb adsorbed/lb adsorbent
x_w	concentration at surface, lb adsorbed/lb adsorbent
X	adsorption term in Equation 26, Sh'_w - Sh
y	gas-phase concentration, lb diffusing species/cu ft
y_b, y_e	gas-phase concentration in bulk of bed, at equilibrium, lb diffusing species/cu ft
y_s, y_w	concentration at saturation, at wall surface
Y	dimensionless group of Equation 3
z	distance taken perpendicular to a flat plate, ft
z_f	thickness of effective laminar gas layer adjacent to surface, ft

Greek

α	shape factor for gamma distribution
β	scale factor for gamma distribution
μ_p	number of particles per square foot of surface
ρ, ρ_p	gas density, particle density
ψ	sphericity, $\pi D_p^2/a_{ext}$
σ	ψ/ϕ
ϕ	surface area factor, $(6/a\rho_p D_p)^{1/2}$

Superscripts

*	indicates pseudo-equilibrium value of gas-phase concentration

II. Introduction

Parts A and B of this work have described work involving simultaneous heat and mass transfer from a spherical surface to a bed of non-adsorbing particles. Attention has been given to the heat transport theory. It is the purpose of this section (Part C) to develop the mass transfer aspect of the work.

There has been considerable study of forced-convection mass transfer to a fluid stream flowing past the outside of a single sphere. Griffith[4] has given a comprehensive summary of the work in this area.

As the particles employed in the fluidized-bed experiments of Parts A and B do not adsorb the diffusing species (water molecules) to any appreciable extent, the mass transfer from the sphere may be considered to occur in the continuous gas phase. If the two cases (i.e., those with and those without fluidized particles) are studied at the same average gas velocity, the differences in their mass transfer properties can be associated with the effects of particle motions on the gas-phase transfer. By suitably defining the effect of the particle motions, the equations predicting the Sherwood numbers (or mass transfer coefficients) for the system without fluidized particles present can be extended to the case in which the surface is surrounded by particles. One of the objects of this section will be to determine equations useful for the prediction of Sherwood numbers from a surface to a bed of nonadsorbing fluidized particles.

There has been only one report[15] of experimental work which describes mass transfer from a fixed surface to a bed of fluidized solids. In this work of van Heerden et al., first coke and then Devarda's alloy were fluidized by an air stream in a column whose wall surfaces were coated with a layer of naphthalene. The mass transfer coefficients were measured at different bed temperatures. These coefficients were found to be strongly dependent on the temperature, increasing with decrease in temperature. In their experiments, an additional mode of mass transfer was available which did not exist in the experiments of the present investigation, namely, particle adsorption. Adsorption on solids will depend considerably on the temperature. The capacity of a particle to adsorb molecules increases with decrease in temperature. It is apparent then that the mass transfer coefficient will increase if the capacity of the solid to adsorb is increased. No attempt was made by van Heerden et al., to develop a model which would predict the Sherwood number (or mass transfer coefficient) as a function of bed properties.

Matter may leave a surface and enter a fluidized bed in at least four different ways: 1) continuous gas phase; 2) particle adsorption; 3) wetting; 4) attrition. By properly controlling the surface conditions, 3) and 4) can be made to represent only a small portion of the total; as will be discussed later.

In addition to permitting a determination of the magnitude of the transport in the continuous gas phase, a theoretical model is proposed which describes the mass transfer by particle adsorption. An expression for the overall Sherwood number, which combines the effects of particle and gas phase transport, is then developed, and the predicted values are compared with those obtained from the data of van Heerden et al.

III. Nonadsorbing Particles

Theory

As previously mentioned, a survey of mass transfer by forced convection from the outside of a single sphere has been made by Griffith.[4] The relationship describing the mass transfer at the Reynolds numbers of the present investigation may be described as

$$Sh = 2 + 0.60\ Re^{1/2}\ Sc^{1/3}, \tag{1}$$

which is of a form originally proposed by Froessling[2] on the basis of boundary-layer theory and empiricism, and then modified to its present form by Ranz and Marshall.[14] The first term on the right-hand side of Equation 1 is the limiting value of the Sherwood number for a Reynolds number approaching zero and negligible natural convection (i.e., a motionless fluid). The second term on the right-hand side accounts for forced convection.

For a sphere which is surrounded by a distended bed of particles (i.e., a bed of stationary particles assuming the positions held in a fluidized bed at a given instant of time) the equation for Sherwood number must be modified to take into account bed voidage. This may be achieved by replacing Re in Equation 1 by $Re_e = G_e D_p/\mu$, where $G_e = G/e$. This is not to be confused with any equation for fixed-bed mass transfer, in which cognizance of the "jetting" effect of the gas through the packing is necessary in evaluating the Reynolds number to be used.

If the sphere is surrounded by fluidized particles, however, in addition to the effect of bed voidage on the superficial gas velocity, some effect of particle motions on the value of Sh should be expected. In the experiments of this investigation adsorption by the particles was negligible (statement verified later) and its effect on Sh small. Conceivably, another term might be added to Equation 1, with Re_e replacing Re, to describe particle motion, and hence mixing of the gas adjacent to the surface. The factors which have an effect on particle motion may be put into a form suitable for dimensional analysis, such as

$$\Phi(Y) = \Phi(\psi, D_p, (\rho_p - \rho), \rho, g, \mu, G_e - (G_e)_{mf}) = \text{constant}. \tag{2}$$

Application of such an analysis to this function of variables, which represents particle motions, results in

$$Y = \frac{\left[G_e - (G_e)_{mf}\right] \mu}{(\psi D_p)^2 (\rho_p - \rho) \rho g} \tag{3}$$

Equation 1 may then be expanded to the following form

$$Sh = 2 + 0.60\ Re_e^{1/2}\ Sc^{1/3} + vY^n; \qquad G > G_{mf}, \tag{4}$$

for use in mass transfer from a sphere to a fluidized bed of particles. The constants v and n are to be determined experimentally.

If the substitution $Sh_e = 2 + 0.60\ Re_e^{1/2}\ Sc^{1/3}$ is made, Equation 4 becomes

$$Sh = Sh_e + vY^n; \qquad G > G_{mf}. \tag{5}$$

It should be noted that the group Y is based on the average diameter of the fluidized particles, whereas Sh is based on the characteristic dimension D_w of the transfer surface (in the case of the sphere, its diameter, D_s). When G_e is decreased to the value for minimum fluidization (the value below which no particle motion exists), Y becomes equal to zero and the Sherwood number is reduced to the value for a distended bed. Although Equation 5 was developed for a spherical surface, it is possible to use it to describe the transfer from any shape of surface providing the value for the Sherwood number Sh_e which pertains to that particular surface is known. The appropriate Sherwood numbers under different flow conditions are given in Table 1. The values for v and n may vary for different surfaces owing to possible variations in particle motion at surfaces of different shape.

IV. Experimental Results

Experimental runs in beds without fluidized particles agreed well with Equation 1, as mentioned in Part A. The experimental results and fluidized-particle properties for the fluidized bed runs of Parts A and B are given in Table 2. The sphericity factor, ψ, is obtained from Brown and Associates[1] as a function of normal packing porosity (void fraction of stationary bed). It is used as an indication of particle shape and is equal to unity for a spherical particle.

To determine the constants v and n in Equation 5, $Sh - Sh_e$ values were, with the corresponding values of Y, put to a least-squares analysis. Runs 2, 3, and 4 for glass and 3 for nickel were omitted from the analysis. The rejected runs with glass particles were found to exhibit static-charge effects. In runs with glass after the first, particles were observed coating the Lucite column and the transfer sphere surface. The layer of stationary particles on the sphere is thought to reduce the effect of particle motion; as a result, little improvement in Sherwood number was possible. Run 3 for nickel was omitted on the basis of its being inconsistent with other measurements with the same particles. By use of the results of the remainder of the runs, the values $n = 0.40 \pm 0.03$ and $v = 33.7 \pm 2.5$

Part C
Table 1

SHERWOOD NUMBERS FOR FORCED-CONVECTION MASS TRANSFER

Flow Direction and Profile	Sh_e	Characteristic Length, D	Re_e Range	Original Source
Sphere →	$2 + 0.60\ Re_e^{1/2}\ Sc^{1/3}$	Diameter	0-1.000	(2,14)
	$0.43\ Re_e^{1/2}\ Sc^{1/3}$	Diameter	400-100,000	(17)
Flat Plate →▬	$0.67\ Re_e^{1/2}\ Sc^{1/3}$*	Length in Flow Direction	<100,000	(13)
Cylinder →	$0.23 + 0.43\ Re_e^{1/2}$	Diameter	0.1-1,000	(11)
	$0.60\ Re_e^{1/2}$	Diameter	1,000-50,000	(11)
Cylindrical Tube (Flow Inside)	$0.023\ Re_e^{0.83}\ Sc^{1/3}$	Diameter	1,800-30,000	(10,3)
Cylinder →□	$0.67\ Re_e^{1/2}\ Sc^{1/3}$	Length in Flow Direction	<60,000	(7)
	$0.0280\ Re_e^{0.80}$		>100,000	(7)
	$Sh_e = BRe^{z}$**			
	z / B			
→◇	0.588 / 0.222	Diameter of Circular Tube of Equal Exposed Surface	5,000-100,000	(5)
→⬭	0.612 / 0.224		2,500-15,000	(9)
→◇	0.624 / 0.261		2,500-7,500	(9)
→⬡	0.638 / 0.138		5,000-100,000	(5)
→⬡	0.638 / 0.144		5,000-19,500	(5)
→□	0.675 / 0.092		8,000-100,000	(5)
→□	0.699 / 0.160		2,500-8,000	(9)
→I	0.731 / 0.205		4,000-15,000	(9)
→⬡	0.702 / 0.035		19,500-100,000	(5)
→○	0.804 / 0.085		3,000-15,000	(9)

*Theoretical
**Table from Ref. (8).

Part C
Table 2

EXPERIMENTAL RESULTS

Material Used	Run	G, lb/(hr)(ft²)	e_s	G_e, lb/(hr)(ft²)	Sh_e	Sh	$D_p^2 \times 10^9$, ft²	ρ_p, lb/ft³	ψ	$G_e - (G_e)_{mf}$	$Y \times 10^3$
Fused Alumina A	1	72.3	0.689	104.9	6.90	9.68	230	243	0.59	40	2.80
	2	92.6	0.733	126.3	7.40	12.55	230	243	0.59	61	4.28
	3	108.9	0.776	140.0	7.70	12.50	230	243	0.59	75	5.26
	4	124.7	0.784	159.0	8.04	14.17	230	243	0.59	94	6.59
	5	145.6	0.796	182.9	8.49	14.04	230	243	0.59	118	8.25
Fused Alumina B	1	92.5	0.722	128.0	7.38	13.57	84	243	0.58	102	20.2
	2	108.9	0.751	144.6	7.72	15.52	84	243	0.58	118	23.4
	3	124.7	0.763	163.0	8.06	15.92	84	243	0.58	137	27.2
Copper (Granules)	1	70.0	0.532	131.7	7.48	12.28	37	559	0.89	77	6.49
	2	108.9	0.632	172.2	8.26	13.16	37	559	0.89	118	9.85
	3	142.2	0.643	221.2	9.06	15.71	37	559	0.89	167	14.0
	4	145.6	0.644	226.3	9.16	15.11	37	559	0.89	172	14.3
Glass	1	72.3	0.570	126.9	7.40	13.70	145	154	0.88	83	9.10
	2	92.6	0.618	150.0	7.86	11.35	145	154	0.88	106	11.6
	3	108.9	0.669	162.7	8.09	9.48	145	154	0.88	109	12.0
	4	124.7	0.678	183.8	8.49	10.63	145	154	0.88	140	15.4
Copper (Spheres)	1	45.2	0.378	119.5	7.24	8.80	210	559	1.00	51	0.594
	2	67.0	0.495	135.2	7.56	9.06	210	559	1.00	66	0.778
	3	86.2	0.536	160.8	8.07	10.35	210	559	1.00	92	1.07
Nickel (Spheres)	1	45.2	0.378	119.5	7.24	8.57	210	555	1.00	51	
	2	67.0	0.464	144.9	7.76	9.39	210	555	1.00	76	0.887
	3	88.6	0.556	159.2	8.05	11.90	210	555	1.00	90	1.05
	4	108.6	0.603	180.1	8.45	10.72	210	555	1.00	111	1.30
Solder (Spheres)	1	45.2	0.328	119.5	7.24	8.54	210	554	1.00	51	0.598
	2	61.0	0.495	135.2	7.56	9.34	210	554	1.00	66	0.774
	3	88.6	0.556	159.2	8.05	11.01	210	554	1.00	90	1.05
	4	124.7	0.603	206.2	8.90	10.80	210	554	1.00	137	1.61
	5	140.0	0.610	229.3	9.25	12.10	210	554	1.00	160	1.88

were predicted, and an average standard deviation of 16.5% was found. Since one relatively large number has been subtracted from another (i.e., Sh - Sh_e) to determine the effect of particle motion, this deviation is surprisingly small.

The deviation in the values of Sh predicted from Equation 5 and the experimental values will be considerably less. This can be seen from Figure 1. The Sherwood numbers were calculated from Equation 5 through use of the values of n and v evaluated from the experiment, that is,

$$Sh = Sh_e + 33.7\ Y^{0.40}; \qquad G > G_{mf}. \tag{6}$$

Only two values have an error greater than 10 percent, and these are only slightly greater. Equation 6 has been verified for $93.4 < Re_e < 201.8$ and $0.594 < Y \times 10^3 < 27.2$. It is expected that the useful Re_e range might be extended to that at which the appropriate Sh_e is valid (see Table 1). However, the validity of this last statement should be verified by experiment.

Part C
Figure 1

AGREEMENT OF EQUATION 6 WITH DATA

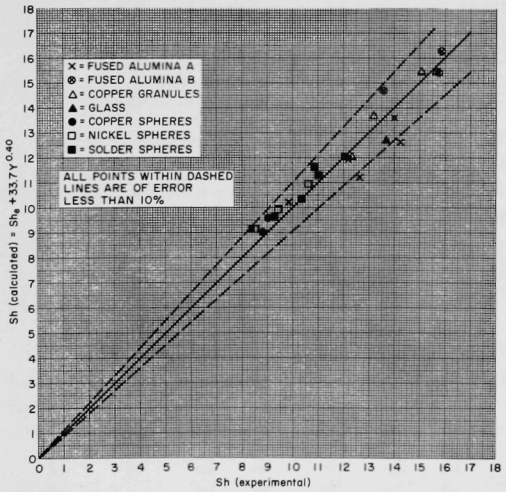

108-6709

The fact that Sh increases with increase in Y is useful in determining the effect of bed properties on mass transfer. For instance, an increase in average particle size will reduce mass transfer as will an increase in particle density. The value of Y, and hence of Sh, decreases with increase in sphericity. Possibly a particle of spherical shape (because of its low surface area-to-volume ratio) will disturb the gas layer less during a rotation than will a nonspherical particle.

There may be variation in the effects of particle motion as described by the term containing Y in Equation 6 with different internal surfaces. However, when Equation 6 with the appropriate Sh_e value was compared with data from a vertical flat plate in a fluidized bed,[6] agreement within 15% was obtained. The variation might be caused by the different mixing patterns experienced by the particles along a vertical flat plate than about

the surface of a sphere. The calculated values were always low for the flat plate, and this would indicate a greater mixing contribution along flat plates than that given in Equation 6 for spheres.

V. Adsorbing Particles

Theory

A model is proposed which predicts the mass transfer coefficients from surfaces to fluidized beds. A particle is visualized entering the gas laminar layer adjacent to the fixed transfer surface, the gas being at the vapor concentration of the diffusing species, y_w, in equilibrium with the adsorbed quantity on the surface, x_w. It is assumed that the particle concentration as it enters the laminar layer is that of the bulk of the bed, x_b. While residing at the surface, the concentration of the adsorbed material on the particle continually increases and may be denoted by the variable x_v at any instant of time. The particle then returns to the bulk of the bed, where it releases the adsorbed species to the incoming gas phase until it reaches its equilibrium concentration, x_b.

Let m be the number of lb/hr diffusing to (or from) a fluidized solid particle. Then,

$$m = \rho_p C_{Tp} v_p \frac{dy_v^*}{dt}, \tag{7}$$

in which ρ_p and v_p are effective particle density and volume, respectively, and y_v^* is the concentration which would be in equilibrium with x_v if true equilibrium existed. Here, C_{Tp} is the "mass capacity" at constant temperature:

$$C_{Tp} = \left(\frac{\partial x_v}{\partial y_v^*} \right)_T ;$$

it represents the number of pounds of material which must be adsorbed by one pound of adsorbent to increase y_v^* by one pound per cubic foot.

Also, it is convenient to assume that diffusion to (or from) the particles occurs according to the equation

$$m = k_c a_p (y_w - y_v^*), \tag{8}$$

in which k_c is an overall mass transfer coefficient and a_p is the particle surface area.

Combination of Equations 7 and 8 results in

$$C_{Tp} \frac{dy_v^*}{dt} = k_c a(y_w - y_v^*), \tag{9}$$

in which a is the BET surface area, equal to $a_p/\rho_p v_p$. This area is readily measureable (see, for instance, Orr and Dallavale[12] for tabulation of a values and methods of evaluation). Integration of Equation 9 over an interval of time t, gives

$$y_w - y_v^* = (y_w - y_b)\, e^{-k_c a t / C_{Tp}}, \tag{10}$$

in which y_b is the concentration of diffusing species in the bulk of the gas and is assumed to be the concentration y_v^* when the particle initially enters the gas laminar layer adjacent to the surface, as there is a high degree of mixing in a fluidized bed. This quantity may be assumed equal to the exit gas concentration and in equilibrium with the solid concentration, x_b.

Application of the result of Equation 10 to Equation 8 gives

$$m(t) = k_c a_p (y_w - y_b)\, e^{-k_c a t / C_{Tp}}, \tag{11}$$

in which m(t) is the flux of material diffusing to a particle at time t. This equation is directly analogous with Equation 1 of Part B. Its derivation is similar to that of Equation 1, derived on the basis that temperature gradients within the particle are negligible (see paragraph following Equation 1, Part B).

To obtain the average weight adsorbed per fluidized-bed particle, it is necessary to assume a distribution of residence times. As mentioned in Part B, it is convenient to use the gamma distribution for many reasons:

$$f(t) = \left(\frac{1}{\alpha! \beta^{\alpha+1}} \right) t^{\alpha} e^{-t/\beta}. \tag{12}$$

Then

$$\overline{m} = \int_0^{\infty} m(t)\, f(t)\, dt = \frac{k_c a_p (y_w - y_b)}{\left[1 + \frac{k_c a \overline{t}}{C_{Tp} (\alpha+1)} \right]^{\alpha+1}}, \tag{13}$$

in which $\overline{m}$ is the time-averaged mass flow of the diffusing species to (or from) the particle.

A mass balance is now set up in the following form:

$$k_w(y_w - y_b) = \mu_p \overline{m} + k_g(y_w - y_b), \tag{14}$$

in which k_w is the experimentally measured surface mass transfer coefficient in beds of adsorbing particles, k_g is the coefficient for mass transfer through the continuous gas phase, and μ_p is the number of adsorbing particles per unit area of surface. If the value of $\overline{m}$ given by Equation 13 is used, Equation 14 may be put in the form

$$k_w = \frac{\mu_p k_c a_p}{\left[1 + \frac{k_c \overline{at}}{C_{Tp}(\alpha + 1)}\right]^{\alpha+1}} + k_g. \tag{15}$$

$\underline{k_c}$

The value of k_c to be used in Equation 15 is taken as the limiting value for adsorption upon a particle in still air (i.e., zero gas velocity and no free convection). The assumption of zero gas velocity in the laminar boundary layer of the gas at the surface is reasonable. Since the particle may be nonspherical and vesicular, the value of k_c described in Appendix C for the nonporous sphere is not applicable.

To obtain a value of k_c for porous materials it is convenient to handle the mass transfer equations by a procedure similar to that used for a sphere in Appendix C, but making appropriate changes. It is necessary to have the equations take into account the effect of available surface area.

For porous particle it is possible to characterize the particle surface by a "surface area factor"

$$\phi^2 = \pi D_s^2 / a_p \tag{16}$$

in which πD_s^2 is the surface area of a sphere of volume equal to that of the given particle. Always ϕ^2 is less than one, and only equals unity for the case of a nonporous sphere.

The diameter of a sphere having the same surface area as the particle is $\sqrt{a_p/\pi}$ or, from Equation 16, D_s/ϕ (the corresponding radius is R_s/ϕ). The gas-phase heat transfer is considered to extend outward from this radius of a sphere of equivalent surface area. Then, following the procedure employed in Appendix C,

$$m = a_p k_c (y_\infty - y_e) = -D_v (4\pi r^2) \frac{dy_g}{dr}$$

and

$$\frac{k_c a_p}{4\pi D_v} \int_{R_s/\phi}^{(R_s/\phi)+\delta} \frac{dr}{r^2} = -\frac{1}{y_\infty - y_e} \int_{y_e}^{y_\delta} dy_g.$$

Finally,

$$\lim_{\delta \to \infty} Sh' = \frac{k_c D_p}{D_v} = \frac{2\pi D_p D_s}{\phi a_p} = \frac{2\sqrt{\pi} D_p}{a_p^{1/2}}, \tag{17}$$

in which D_p is the average diameter of a particle (given by screen analysis). For spherical particles which are nonporous, $D_s = D_p$; $a_p = \pi D_s^2$; and $\phi = 1$; therefore, $Sh' = 2$.

For a flat plate of infinite extent, $a_p \to \infty$. Therefore, $Sh' = 0$. These two special results confirm the values determined individually in Appendix C.

Replacement of a_p by $\pi D_s^2/\phi^2$ in Equation 17 results in

$$Sh' = 2\phi D_p / D_s. \tag{18}$$

For most fluidized bed particles the assumption $D_s \approx D_p$ is valid (see Appendix C for test of this assumption in the case of coke, a vesicular solid). Then Equation 18 reduces to the simple form

$$Sh' = 2\phi. \tag{19}$$

The value of k_c appropriate for use in Equation 15 is then $k_c = 2\phi D_v / D_p$. It might be noted that when $D_p = D_s$, Equation 16 becomes

$$\phi^2 = \frac{\pi D_p^2}{a \rho_p \left(\frac{\pi D_p^3}{6} \right)} = \frac{6}{a \rho_p D_p}. \tag{20}$$

Therefore, the surface area factor may be calculated from measurable quantities: BET area, density, and average particle diameter.

μ_p

The value of μ_p is assumed to be that for spheres of projected diameter D_a (the diameter of a sphere having the same external area, a_{ext}, as the particle). Spheres of diameter D_a are assumed to be hexagonally packed along the wall surface, as in Figure 2. The triangle represents the repeating section; from it the ratio of projected particle area to wall surface area may be calculated. The total projected particle area within the triangle is $\pi D_a^2/2$. Then it follows that

$$\frac{\text{projected particle area}}{\text{surface area}} = \frac{\pi D_a^2/2}{\sqrt{3}\, D_a^2} = \frac{\pi}{2\sqrt{3}}.$$

The projected area per particle is $\pi D_a^2/4$. Therefore,

$$\mu_p = \frac{\text{no. particles}}{\text{surface area}} = \frac{\pi/2\sqrt{3}}{\pi D_a^2/4} = \frac{2}{\sqrt{3}\, D_a^2}. \tag{21}$$

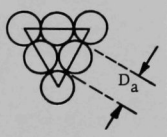

Part C
Figure 2
EVALUATION OF NUMBER OF PARTICLES PER UNIT SURFACE AREA

The sphericity, ψ, previously mentioned in connection with the Y factor for particle motion, is defined as the ratio of the surface area of a sphere having the same volume as a given particle to the external area (that portion of a particle surface encountering the flow). Therefore,

$$\psi = \pi D_p^2/a_{ext} = \pi D_p^2/\pi D_a^2. \tag{22}$$

Here, D_p is again substituted for D_s, and the value of a_{ext} follows from the definition of D_a. The range of ψ for most fluidized-bed particles is from 0.5 to 1.0, with unity as the value for a spherical particle. The value of D_a obtained from Equation 22 is then substituted into Equation 21 with the result that

$$\mu_p = 2\psi/\sqrt{3}\, D_p^2, \tag{23}$$

which may now be employed in Equation 15. With $\psi = 1$ for spherical particles, the value of μ_p as used in Part B is obtained.

It is informative to compare the sphericity, ψ, with the surface area factor, ϕ^2. The sphericity is a measure of the external shape in comparison with that of a sphere of the same volume, whereas the surface

area factor is a measure of the total (internal and external) surface as compared with that of a nonporous sphere of the same volume. The sphericity is, therefore, determined by measuring external properties, such as effective bed voidage [see, for example, Brown and Associates[1]]. The surface area factor, on the other hand, is obtained from the measurement of total surface properties, such as BET surface area (see Equation 20). To make the distinction even clearer, it might be stated that a porous sphere will have a ψ value of unity but a ϕ^2 value less than unity owing to additional internal surface area. However, a nonporous sphere will have values of both ψ and ϕ equal to one.

Insertion of the proper values derived for k_c and μ_p into Equation 15, and use of the value $\alpha = 1$, which was the optimum as determined from the heat transfer experiments (see Part B), yields the following result:

$$Sh'_w = \frac{4\pi/\sqrt{3}\ \sigma}{\left[1 + \dfrac{6D_v\bar{t}}{\phi D_p^2 \rho_p C_{Tp}}\right]^2} + Sh', \tag{24}$$

in which $\sigma = \phi/\psi$.

For nonporous spherical particles, $\sigma = \phi = 1$, and Equation 24 reduces to a form which is analogous to that of Equation 8a in Part B. The "primes" on the Sherwood numbers indicate that the characteristic dimension of length is that of the particle (i.e., its diameter), and not of the wall or fixed surface. To convert unprimed to primed Sherwood number, use is made of the equation

$$Sh' = (D_p/D_w)\ Sh. \tag{25}$$

The values of Sh are obtained from Equation 5. Sh' represents the transfer through the pure gas phase which is being mixed by the moving particles. The first term on the right-hand side of Equation 24 represents the contribution to the overall Sherwood number, Sh'_w, via particle adsorption.

C_{Tp}

The mass capacity of a solid adsorbent for a species in the gas phase has been defined earlier. The property may be evaluated from equilibrium data (y_e vs x_e) at the temperature of the system. van Heerden, et al.[16] have obtained such equilibrium information for the air-naphthalene system with coke and Devarda's alloy as adsorbents. This was accomplished by passing a known concentration of naphthalene vapor in air mixture through a given weight of fluidized particles. By a continuous analysis of the exit gas concentration, the amount adsorbed was known as a

function of time. The outlet concentration was assumed to be in equilibrium with the concentration adsorbed on the particles. This assumption was justified by van Heerden by means of an analogy with heat transfer: "Just as the high heat capacity of the circulating particles establishes a constant temperature throughout the bed, the relatively high adsorption capacity of the particles maintains a constant naphthalene concentration." Curves of y_e vs x_e varied significantly with change in the isotherm temperature. However, by plotting values of partial saturation y_e/y_s vs x_e, the variation with temperature as parameter was considerably reduced. The linear portion of two isotherms for coke and one for Devarda's alloy as obtained by van Heerden et al. are given in Figure 3.

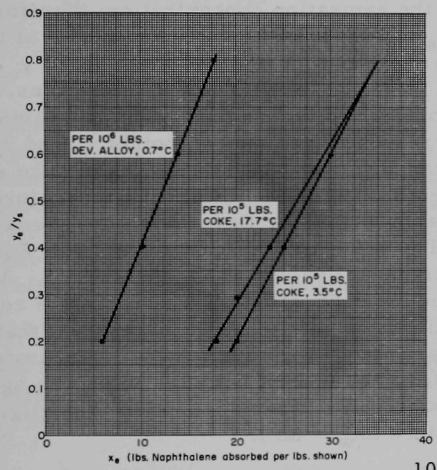

108-6710

Part C
Figure 3

EQUILIBRIUM CURVES FROM DATA OF VAN HEERDEN

From the definition given earlier for mass capacity of a particle,

$$C_{Tp} = \left(\frac{\partial x_e}{\partial y_e}\right)_T,$$

which is to be evaluated at the y_e or x_e for which C_{Tp} is desired. To obtain C_{Tp} from Figure 3, this equation may be put into the form

$$C_{Tp} = \left(\frac{\partial x_e}{\partial\left(\frac{y_e}{y_s}\right)}\right)_T \frac{1}{y_s} = \frac{(\text{slope})^{-1}}{y_s}. \qquad (26)$$

VI. Agreement of Theory with Data

In addition to the equilibrium isotherm studies, van Heerden et al.[16] have measured mass transfer coefficients from a surface to a bed of adsorbing particles. In these experiments, naphthalene was coated on the inner wall of a cylindrical column instead of entering with the inlet air stream. Values calculated from the data of these experiments for the purpose of testing the applicability of Equation 24 are given in Table 3. The C_{Tp} values are obtained from Figure 3 and Equation 26. The values reported are the average of those at the bulk y_b and mean film y_f^* concentrations. As the wall is completely coated with naphthalene, it is assumed that the gas concentration associated with it is the saturation concentration; therefore, $y_w = y_s$. Most of the values of y_b/y_s and y_f^*/y_s lie in the linear region of the equilibrium curve. The slope of the curve of Figure 3 and the value of y_s at these partial saturation values will, therefore, be constant for most runs, and consequently C_{Tp} is the same at both y_b and y_f^*. In the nonlinear region, slope values must be computed corresponding to the two points y_b and y_f^*; the resulting C_{Tp} values are then averaged. In evaluating the C_{Tp} of coke some interpolation (extrapolation) was necessary for the different temperatures of the runs. No such compensation was possible for Devarda's alloy, because only one isotherm was available. The values of Sh'_w calculated from Equation 24 are compared with the experimental values of Sh'_w in Table 3. Approximate values of Sh' are obtained from Equation 6. The reader is referred to Appendix C for all pertinent calculations. It is apparent that the equation developed for adsorbing particles (i.e., Equation 24) is accurate only at the higher adsorbing rates for each type of particle, with less agreement for the cases of lower adsorption rates (when adsorption is negligible good agreement is again obtained since $Sh'_w \rightarrow Sh'$).

Part C
Table 3

COMPARISON OF EQUATION 24 AND DATA OF VAN HEERDEN ET AL.[16]

	Temp, °C	$y_s \times 10^6$, lb/ft³	$y_b \times 10^6$, lb/ft	$y_f^* \times 10^6$, lb/ft	$\frac{y_b}{y_s}$	$\frac{y_f^*}{y_s}$	C_{Tp}, ft³/lb	D_V, ft²/hr	Sh', calc by Eq. 6	Sh'_w, calc by Eq. 24	Sh'_w, exptl
Coke	5.1	4.68	3.37	4.02	0.72	0.86	58.9	0.214	0.03	1.24	1.47
	13.0	10.60	6.24	8.4	0.59	0.80	27.2	0.224	0.03	0.36	0.84
	14.8	13.1	8.10	10.6	0.60	0.81	22.0	0.226	0.03	0.25	0.81
	26.2	39.2	17.5	28.7	0.45	0.73	7.90	0.242	0.03	0.06	0.43
	31.1	64.9	23.7	44.3	0.37	0.69	5.02	0.247	0.03	0.04	0.31
	33.0	75.5	20.0	47.6	0.26	0.63	4.40	0.250	0.03	0.03	0.19
Devarda's Alloy	6.4	5.43	1.56	3.5	0.29	0.65	3.61	0.216	0.023	0.31	0.31
	13.2	11.2	3.12	7.2	0.27	0.64	1.75	0.224	0.023	0.10	0.24
	20.5	61.0	10.0	35.5	0.16	0.58	0.40	0.247	0.023	0.027	0.12
	42.5	168.0	16.8	92.5	0.10	0.55	0.15	0.263	0.023	0.024	0.06

A possible explanation for the deviation from the predicted model is attributed to the increased error in the assumed value of μ_p as the adsorption decreases. The effective gas laminar region includes in these

instances a considerably greater number of particles than would be present in a single layer of particles as was assumed. The thickness of the gas laminar layer may be written as

$$z_f = D_v(y_s - y_b)/m',$$

where m' is some average flux into the gas phase. The value of m' is assumed (consequences of this assumption are discussed below) to vary linearly with the mass velocity of the gas. Therefore,

$$\frac{z_f}{D_p} \propto \frac{D_v (y_s - y_b)}{D_p G}. \qquad (27)$$

Proportionality 27 is a measure of the number of particle layers within the laminar gas layer and, hence, is indicative of the deviation from the assumption of a single particle layer used to calculate μ_p. It might be pointed out justifiably that m' is not proportional to G as was assumed. However, G was a constant in all runs and therefore serves only to make the group of which it is a part in Proportionality 27 dimensionless. If m' is any function of G other than a linear one as assumed, it would only have the effect of changing the constant of proportionality.

In order to isolate the effect of an error in μ_p it is convenient to label the group on the right-hand side of Equation 24 (that containing μ_p) X. A value of X may be determined from the experimental Sherwood number Sh'_w by the expression

$$X_{exp} = Sh'_{w_{exp}} - Sh'.$$

The ratio of X_{calc}/X_{exp} is plotted in Figure 4 as a function of $D_v(y_s - y_b)/D_pG$ to ascertain any possible systematic deviation in the calculated X value. It can be seen that the best agreement occurs for both systems at the lowest values of $(y_s - y_b)D_v/D_pG$. This indicates that best results are obtainable for the case in which the number of effective particle layers is smallest, and hence those cases for which the assumptions involved in the derivation of μ_p are most likely to be correct.

As the value of $(y_s - y_b)D_v/D_pG$ increases, the value of Sh'_w approaches Sh'. In van Heerden's experiments Sh'_w most closely approached Sh' for Devarda's alloy at 42.5°C, which corresponds to the highest value of $(y_s - y_b)D_v/D_pG$, namely, 1.05×10^{-4}. The values of this group evaluated for the particles discussed in the section entitled "Nonadsorbing Particles" were typically of the order 10^{-2}. This lends justification to neglect of the effects of gas adsorption on those particles.

Part C
Figure 4

DEVIATION IN X AS A FUNCTION OF $(y_s - y_b)D_v/D_pG$

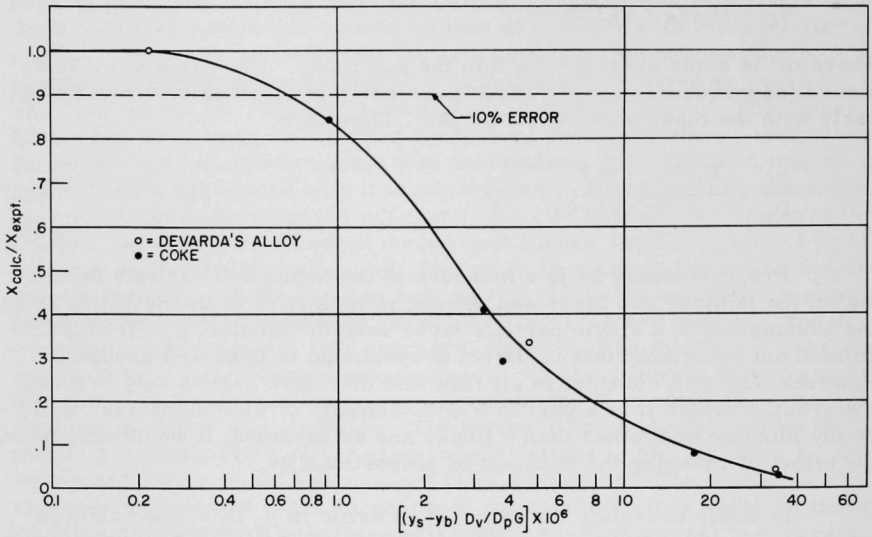

In summary, it might be stated that equations are developed for predicting with good accuracy Sherwood numbers for nonadsorbing particles (see Equation 5) and highly adsorbing particles (see Equation 24). Under intermediate conditions of adsorption, deviations of the predicted Sherwood numbers from the experimental values occur which are found to be related to the group $(y_s - y_b)D_v/D_pG$.

LITERATURE CITED - PART A

1. Botterill, J. S. M., Brit. Chem. Eng., 8, 21 (1963).

1a. Botterill, J. S. M., Redish, K. A., Ross, D. K., and Williams, J. R., Proc. of the Sympos. on Interaction between Fluids and Particles, London (June 1962).

2. Chilton, T. H., and Colburn, A. P., Ind. Eng. Chem., 26, 1183 (1934).

3. Dow, W. M., and Jakob, M., Chem. Eng. Prog., 47, 637 (1951).

4. Ernst, R., Chem.-Ing.-Tech., 31, 166 (1959).

5. Froessling, N., Gerlands Beitr. Geophys., 52, 170 (1938).

6. General Electric Company, Dew Point Recorder Pamphlet, GEI-40444A.

7. Griffin, R. M., Chem. Eng. Sci., 12, 198 (1960).

8. Leva, M., Paper presented at General Discussion of Heat Transfer, London (Sept 1951).

9. Leva, M., and Grummer, M., Ind. Eng. Chem., 40, 415 (1948).

10. Leva, M., Weintraub, M., and Grummer, M., Chem. Eng. Prog., 45, 563 (1949).

11. Mickley, H. S., and Fairbanks, D. F., A.I.Ch.E. Journal, 1, 374 (1955).

12. Mickley, H. S., Fairbanks, D. F., and Hawthorn, R. D., Chem. Eng. Prog. Symp. Series No. 32 (1961).

13. Mukhlenov, I. P., Traber, D. G., Sarkits, V. B., and Bondarchuck, T. P., Zhur. Priklad. Khim. 32, No. 6, 1291 (1959).

14. Ranz, W. E., and Marshall, W. R., Jr., Chem. Eng. Progr., 48, 141, 173 (1952).

15. Sarkits, V. B., Traber, D. G., and Mukhlenov, I. P., Zhur. Priklad. Khim., 32, No. 10, 2218 (1959).

16. Ibid., Zhur. Priklad. Khim., 33, No. 10, 2197 and 2206 (1960).

16a. Short, W. W., Brown, R. A. S., and Sage, B. H., J. Appl. Mech., 27, 393 (1960).

17. Thodos, G., Northwestern University, Evanston, Illinois, Personal Communication.

18. van Heerden, C., Nobel, A. P. P., and van Krevelen, D. W., Ind. Eng. Chem., 45, 1237 (1953).

19. Ibid., Chem. Eng. Sci., 1, No. 2, 51 (1951).

20. Vreedenberg, H. A., J. Appl. Chem., 2, Supplementary Issue No. 1 (1952).

21. Ibid., Chem. Eng. Sci., 11, 274 (1960).

22. Wen, Chin-Yung, and Leva, Max, A.I.Ch.E. Journal 2, 482 (1956).

23. Wender, L., and Cooper, G. T., A.I.Ch.E. Journal, 4, 15 (1958).

24. Wicke, E., and Fetting, F., Chem.-Ing.-Tech., 26, 301 (1954).

25. Wicke, E., and Hedden, K., Chem.-Ing.-Tech., 24, 82 (1952).

26. Zenz, F. A., and Othmer, D. F., Fluidization and Fluid Particle Systems, Reinhold Publ. Co. (1960).

LITERATURE CITED - PART B

1. Baerg, A., Klassen, J., and Gishler, P. E., Can. J. Res., 28, 287 (1950).

2. Baddour, R. F., and Yoon, C. Y., Chem. Eng. Prog. Symp. Ser., 57, No. 32, 35 (1961).

3. Botterill, J. S. M., and Williams, J. R., Trans. Inst. Chem. Engrs., 41, 217 (1963).

4. Botterill, J. S. M., Redish, K. A., Ross, D. K., and Williams, J. R., Proceedings of the Symposium on Interaction between Fluids & Particles, London (June 1962).

5. Brotz, W., Chem.-Ing.-Tech., 28, 165 (1956).

6. Brusenback, R. A., Ph.D. Thesis, Northwestern University, Evanston, Ill. (June 1963).

7. Carslaw, H. S., and Jaeger, J. S., Conduction of Heat in Solids, Oxford University Press, London (1959).

8. Dow, W. M., and Jakob, M., Chem. Eng. Prog., 47, 637 (1951).

9. Ernst, R., Chem.-Ing.-Tech., 31, 166 (1959).

10. Froessling, N., Gerlands Beitr. Geophys., 52, 170 (1938).

10a. Jakob, A., and Osberg, G. L., Can. J. Chem. Eng., 35, 15 (1957).

11. Leva, M., Weintraub, M., and Gummer, M., Chem. Eng. Prog., 45, 563 (1949).

12. Levenspiel, O., and Walton, J. S., Chem. Eng. Prog. Symp. Ser. No. 9 (1954).

13. Levenspiel, O., and Walton, J. S., Heat Transfer and Fluid Mechanics Symposium, Berkeley, Calif. (1949).

14. Mickley, H. S., Fairbanks, D. F., and Hawthorn, R. D., Chem. Eng. Prog. Symp. Ser. 57, No. 32, 51 (1961).

15. Mickley, H. S., and Fairbanks, D. F., A.I.Ch.E.J., 1, 374 (1955).

16. Mickley, H. S., and Trilling, C. A., Ind. Eng. Chem., 41, 1135 (1949).

17. Miller, C. O., and Logwinuk, Ind. Eng. Chem., 43, 1220 (1951).

18. Mukhlenov, I. P., Traber, D. G., and Sarkits, U. B., Zhurn. Prik. Khim., 33, 2206 (1960).

19. Olin, H. L., and Dean, O. C., Petroleum Engineer, p. C-23 (March 1953).

20. Rowe, P. N., and Partridge, B. A., UKAEA Report AERE/R4108 (1963).

21. Toomey, R. D., and Johnstone, H. F., Chem. Eng. Prog. Symp. Ser., 49, 51 (1953).

22. Traber, D. G., Sarkits, V. B., and Mukhlenov, I. P., Zhurn. Prik. Khim., 33, 2197 (1960).

23. van Heerden, C., Nobel, A. P. P., and van Krevelen, D. W., Ind. Eng. Chem. 45, 1237 (1953).

24. van Heerden, C., Nobel, A. P. P., and van Krevelen, D. W., Chem. Eng. Sci., 1, 51 (1951).

25. Vreedenberg, H. A., J. Appl. Chem. (London), 2 (Suppl. Issue 1) S26-S33 (1952).

26. Vreedenberg, H. A., General Discussion on Heat Transfer, Sec. IV, 32, Institution of Mechanical Engineers, London (1951).

26a. Wen, C., and Leva, M., A.I.Ch.E.J. 2, 482 (1956).

27. Wicke, E., and Fetting, F., Chem.-Ing.-Tech., 26, 301 (1954).

28. Ziegler, E. N., Koppel, L. B., and W. T. Brazelton, Ind. Eng. Chem. (to appear in 1964).

LITERATURE CITED - PART C

1. Brown, G. G., Unit Operations, John Wiley & Sons, Inc., New York (1950) p. 214.
2. Froessling, N., Beitrage zur Geophysik von Garland, 52, 170 (1938).
3. Gilliland, E. R., and Sherwood, T. K., Ind. Eng. Chem., 26, 516 (1934).
4. Griffith, R. M., Chem. Eng. Sci., 12, 198 (1960).
5. Hilpert, R., and Torschung, A. D., Geo. D. Ingenierwes., 4, 215 (1933).
6. Holmes, J., Argonne National Laboratory, Personal Communication (1963).
7. Jakob, M., and Dow, W. M., Trans. Am. Soc. Mech. Engrs., 68, 123 (1946).
8. Jakob, M., Heat Transfer, John Wiley & Sons, Inc., New York (1949) p. 562.
9. Knoblavch, O., and Reiher, H. "Waermeuebertragung," in W. Wien and F. Harms, Handbuch d. Experimentalphysik, Vol. 9, p. 313, Footnote.
10. Linton, W. H., and Sherwood, T. K., Chem. Eng. Prog., 46, 258 (1950).
11. McAdams, W. H., Heat Transmission, 3rd Edition, McGraw-Hill Book Co., Inc., New York (1954) p. 260.
12. Orr, C., Jr., and Dallavale, J. M., Fine Particle Measurement, Macmillan Co., New York (1959).
13. Polhausen, E., Z. angew. Math. u. Mech., 1, 115 (1921).
14. Ranz, W. E., and Marshall, W. R., Jr., Chem. Eng. Progr., 48, 141, 173 (1952).
15. van Heerden, C., Nobel, P., and van Krevelen, D. W., Chem. Eng. Sci., 1, 37, 51 (1951).
16. van Heerden, C., Nobel, A. P. P., and van Krevelen, D. W., Ind. and Eng. Chem., 45, 1237 (1953).
17. Williams, G. C., Sc. D. Thesis in Chemical Engineering, Massachusetts Institute of Technology (1942).

APPENDIX A

ERROR CAUSED BY THERMOCOUPLE NOT BEING AT SURFACE

A simple model is chosen to determine the temperature at $\frac{1}{32}$ in. from the surface of the sphere.

The conditions of the problem was as follows: Sphere $0 \leq r < a$; initial temperature, V; constant surface temperature, v_s; temperature at distance r is v.

From Carslaw and Jaeger, Conduction of Heat in Solids, Oxford U. Press (1950),

$$\frac{v - v_s}{V - v_s} = 1 - \frac{a}{\sqrt{\pi \kappa t}} \sum_{n=0} \exp\left[-\frac{(2n+1)^2 a^2}{4\kappa t}\right],$$

where

$$\kappa = \alpha/\rho c_p,$$

v_s is assumed to be constant at the final steady-state value, and V is assumed to be the air temperature.

Let t = 10 min, a typical steady-state value.

It is necessary to carry out the series expansion to n = 27 before terms of second order are reached. At this point

$$\frac{v - v_s}{V - v_s} = 0.050.$$

Carrying out the series to further terms could only reduce this ratio. Therefore, the maximum percent error calculated by this model is 5%. Calculated coefficients would tend to be high from this effect.

Convection of water in the pores and deviations from steady state will reduce the accuracy of this model. Therefore, no attempt was made to correct the temperatures on the basis of this error calculation.

Description of Dew Point Recorder

A small controlled sample is tapped from the exit gas into the dew point instrument. The sample flows into a leak-tight gas chamber having a mirror for one of its walls. The gas is made to flow past this mirror surface. The mirror temperature may be adjusted by a built-in refrigeration system and electrical heating coils. A beam of light is directed at the

mirror and the reflected light is picked up by a photocell unit. If the mirror temperature drops below the dew point, condensation occurs and the light reflection is reduced. The output of the photocell is amplified and controls the heater. Therefore, when condensation commences, heat is supplied to the surface as a consequence of the decrease in photocell pick-up. The temperature then rises slightly above the dew point until the mirror clears. After clearing, refrigeration again occurs. In this manner the photocell "hunts" the dew point. A fine thermocouple constantly records the mirror temperature. The instrument was guaranteed to within 2°F absolute accuracy and was calibrated to give 1°F accuracy.

EXPERIMENTAL DATA

Material	Run	G	e	G_e	G_{mf}	Re	h_c	k_y
No Particles	1	124.7	1.0	-	-	111.0	3.13	11.9
	2	163.2	1.0	-	-	144.2	3.79	15.6
	3	218.0	1.0	-	-	192.2	4.04	17.1
	4	145.6	1.0	-	-	129.6	3.12	12.3
Copper	1	70.0	0.532	131.7	22.2	62.4	34.0	21.4
	2	108.9	0.632	172.2	22.2	96.9	42.8	23.0
	3	145.6	0.644	226.3	22.2	129.6	34.0	26.4
	4	142.2	0.643	221.2	22.2	125.8	36.5	27.4
A-Fused Alumina	1	124.7	0.784	159.0	40.7	111.0	73.3	24.7
	2	145.6	0.796	182.9	40.7	129.6	73.3	24.5
	3	72.3	0.689	104.9	40.7	64.4	40.5	16.9
	4	92.6	0.733	126.3	40.7	82.5	76.0	21.9
	5	108.9	0.776	140.0	40.7	96.9	66.0	21.3
B-Fused Alumina	1	92.5	0.722	128.0	15.7	82.5	62.4	23.7
	2	108.9	0.751	144.6	15.7	96.9	57.9	27.0
	3	124.7	0.763	163.0	15.7	111.0	49.5	27.8
Glass	1	72.3	0.570	126.9	19.7	64.4	100.9	23.9
	2	92.6	0.618	150.0	19.7	82.5	81.1	18.1
	3	108.9	0.669	162.7	19.7	96.9	84.8	16.6
	4	124.7	0.678	183.8	19.7	111.0	100.5	18.6

Material	Run	h'_c	k'_y	(h'_c/k'_y)	h_f	k_y/k'_y	$(h_f-h'_c)/h_c \times 100\%$	h_p	$h_p/h_c \times 100\%$
Copper	1	3.25	13.1	0.247	5.29	1.6	6.0	28.7	84.5
	2	3.62	14.5	0.250	5.76	1.6	5.0	37.0	86.5
	3	4.04	16.1	0.250	6.60	1.6	7.5	27.4	80.6
	4	4.00	15.9	0.251	6.88	1.77	7.9	29.6	81.1
A-Fused Alumina	1	3.51	14.1	0.249	6.15	1.8	3.6	67.1	91.6
	2	3.71	14.9	0.249	6.11	1.6	3.3	67.2	91.6
	3	3.00	12.1	0.247	4.16	1.4	2.9	36.3	89.8
	4	3.21	13.0	0.248	5.42	1.7	2.9	70.6	93.0
	5	3.35	13.5	0.249	5.30	1.6	3.0	60.7	92.1
B-Fused Alumina	1	3.22	13.0	0.249	5.90	1.8	4.3	56.5	90.6
	2	3.37	13.5	0.249	6.73	2.0	5.8	51.2	88.5
	3	3.53	14.2	0.249	6.92	2.0	6.8	42.6	86.2
Glass	1	3.22	13.0	0.248	5.92	1.8	2.7	95.0	94.2
	2	3.43	13.8	0.249	4.51	1.3	1.3	76.6	94.4
	3	3.54	14.2	0.249	4.14	1.2	0.7	80.7	95.2
	4	3.71	14.9	0.249	4.65	1.3	0.9	96.1	95.4

APPENDIX B

	1/2-IN. SPHERE, SIMULTANEOUS HEAT AND MASS TRANSFER			1/2 x 2-1/4-IN. CYLINDER; PURE HEAT TRANSFER	
	G, lb/hr-ft^2	h_c, Btu/hr-ft^2-°F	Mass Transfer Coefficient, lb/hr-ft^2-atm	G, lb/hr-ft^2	h_c, Btu/hr-ft^2-°F
Nickel	13.4	14.9	0.388	13.4	7.4
	20.2	18.5	0.432	20.2	7.4
	45.2	76	0.513	50.5	111
	67.0	98	0.561	67.0	109
	88.6	106	0.717	-	-
	108.9	87	0.642	-	-
Copper	13.4	16.0	0.410	13.4	7.5
	20.2	18.7	0.409	20.2	7.8
	45.2	69	0.526	45.2	96
	67.0	90	0.542	67.0	114
	86.2	99	0.619	86.2	96
Solder	13.4	12.8	0.409	20.2	7.4
	45.2	44	0.510	39.7	34
	67.0	72	0.558	47.9	81
	88.6	77	0.659	68.5	83
	124.7	71	0.645	94.5	81
	140.0	80	0.724	-	-

APPENDIX C

SHERWOOD NUMBERS FOR PARTICLES IN STILL FLUIDS

A. Flat Plate

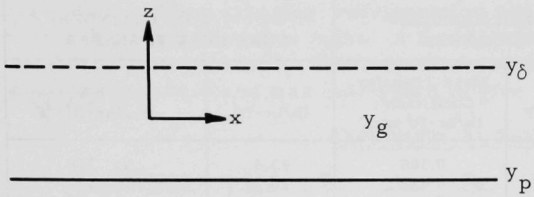

Let

y_g - gas-phase concentration at distance z from surface;

y_δ - gas-phase concentration at distance δ from surface;

y_p - gas-phase concentration at surface of particle.

Then

$$m = k_c(y_\infty - y_p) = -D_v \frac{dy_g}{dz}$$

and

$$\frac{-k_c}{D_v}\int_0^\delta dz = \frac{1}{y_\infty - y_p}\int_{y_p}^{y_\delta} dy_g,$$

where y_∞ is the concentration at an infinite distance from surface. Thus

$$\frac{k_c\delta}{D_v} = \frac{y_\delta - y_p}{y_\infty - y_p};$$

$$Sh_x = \frac{kx}{D_v} = \frac{x}{\delta}\frac{y_\delta - y_p}{y_\infty - y_p};$$

$$\lim_{\delta \to \infty} Sh_x = \lim_{\delta \to \infty} \frac{x}{\delta}\frac{y_\delta - y_p}{y_\infty - y} = 0.$$

B. Sphere

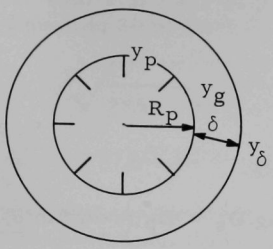

For the spheres

$$m = 4\pi R_p^2 k_c (y_\infty - y_p) = -D_v (4\pi r^2) \frac{dy_g}{dr};$$

$$\frac{-k_c R_p^2}{D_v} \int_{R_p}^{R_p + \delta} \frac{dr}{r^2} = \frac{1}{y_\infty - y_p} \int_{y_p}^{y_\delta} dy_g;$$

$$Sh' = \frac{k_c D_p}{D_v} = \frac{2k_c R_p^2}{D_v (R_p + \delta)} + 2\frac{y_\delta - y_p}{y_\infty - y_p};$$

$$\lim_{\delta \to \infty} Sh' = \lim_{\delta \to \infty} \left[\frac{2k_c R_p^2}{D_v (R_p + \delta)} \right] + \lim_{\delta \to \infty} \left[\frac{2(y_\delta - y_p)}{y_\infty - y_p} \right] = 0 + 2 = 0.$$

ERROR IN ASSUMPTION $D_s = D_p$ FOR COKE

van Heerden et al. (see Ref. 15 of Part C) determined the effective diameter D_e (diameter of spherical particles having the same number of particles per unit volume at maximum porosity of fixed bed as do the actual particles at maximum porosity) of a sphere.

For coke, $D_e = 1.2\ D_p$, for which D_p is the average diameter (screen analysis).

The maximum porosities for a fixed bed are given as $e_{spheres} = 0.406$ and $e_{coke} = 0.564$.

Let

$$n = \text{number of particles per unit volume} = \frac{1 - 0.406}{\pi D_e^3/6} = \frac{1 - 0.564}{v_p}.$$

Therefore

$$v_p = \frac{0.436}{0.594} \times \frac{\pi D_e^3}{6} = 1.25 \left(\frac{\pi D_p^3}{6} \right).$$

By definition,

$$v_p = \pi D_s^3/6.$$

Hence, $D_s = 1.08\ D_p$, or the error in assuming $D_s = D_p$ is within 8%.

In determining the weight of a particle, if the diameter D_p is used as the diameter of a spherical particle (i.e., $v_p = \pi D_p^3/6$), the density must be corrected. For coke, $\rho_p = \rho_s/1.25 = 122.2/1.25 = 96.6$ lb/ft^3.

As Devarda's alloy is relatively nonvesicular and as the necessary D_e was not available, $\rho_p = \rho_s$ was assumed.

CALCULATIONS FOR TABLE 3

Typical calculations of Sh'_w for both coke and Devarda's alloy are given.

Coke at 13.0°C

van Heerden's data:

$$y_s = 10.60 \times 10^{-6};\ y_b = 6.24 \times 10^{-6}\ \text{lb/ft}^3;$$

$$y_f^* = \frac{10.60 \times 6.24}{2} \times 10^{-6} = 8.42 \times 10^{-6}\ \text{lb/ft}^3;$$

$$\frac{y_f^*}{y_s} = 0.80;\quad \frac{y_b}{y_s} = 0.59.$$

As both of these partial saturation values lie on the linear portion of the curve of Figure 3 of Part C, from Equation 26 we obtain:

$$C_{Tp} = \frac{35.25 - 18.00}{0.800 - 0.200} \times \frac{1}{10.60} \times \frac{10^{-6}}{10^{-6}} = 27.2\ \text{lb/lb (lb/ft}^3\text{)}.$$

D_v at 13.0°C = 0.224 ft^2/hr.

$\rho_p = 96.6$ lb/ft^3; $D_p = 2.8 \times 10^{-4}$ ft, a = 2850 ft^2/lb.

t = 1 sec.

The porosity at loosest possible packing is 0.56. From Brown and associates (see Ref. 1 of Part C, p. 214), the corresponding sphericity is ψ = 0.65. From Equation 20 of Part C

$$\phi = \sqrt{\frac{6}{2850 \times 96.6 \times 2.87 \times 10^{-4}}} = 0.275;$$

$$\sigma = 0.275/0.65 = 0.423.$$

An approximate value for Sh may be obtained from Equation 6 by use of the Sh_e corresponding to flow through a cylindrical tube from Table 1:

$$Sh = k_g D_w/D_v = 0.023\ Re_e^{0.83}\ Sc^{0.44} + 33.7\ Y^{0.4}$$

$$= 11.5 + 14.9 = 26.4.$$

Then

$$Sh' = k_g D_p/D_v = \frac{2.87 \times 10^{-4}}{0.288} \times 26.4 = 0.026 \text{ or } 0.03.$$

All the values necessary are now known and may be substituted in Equation 24:

$$Sh'_w = \frac{4\pi/\sqrt{3} \times 0.423}{\left[1 + \frac{6 \times 0.244 \times 1/3600}{0.275 \times (2.87 \times 10^{-4})^2 \times 96.6 \times 27.2}\right]^2} + 0.03$$

$$= 0.33 + 0.03 = 0.36.$$

Devarda's Alloy at 6.4°C

$y_s = 5.43 \times 10^{-6}$;

$y_b = 1.56 \times 10^{-6}$;

$y_f^* = 3.5$; $y_f^*/y_s = 0.65$; $y_b/y_s = 0.29$;

$$C_{Tp} = \frac{17.75 - 6.00}{0.800 - 0.200} \times \frac{1}{5.43} \times \frac{10^{-6}}{10^{-6}} = \underline{3.61}\ \text{lb/lb (lb/ft}^3\text{)};$$

D_v = 0.216 ft²/hr; ρ_p = 336 lb/ft³; $D_p = 3.65 \times 10^{-4}$ ft;

a = 260 ft²/lb; $\bar{t}$ = 1 sec.

The porosity at loosest packing is 0.53; from Brown[1] $\psi = 0.66$.

$$\phi = \sqrt{\frac{6}{260 \times 336 \times 3.65 \times 10^{-4}}} = \underline{0.434.}$$

$$\sigma = 0.434/0.66 = 0.656.$$

$$Sh = k_g D_w / D_v = 11.5 + 6.3 = 17.8.$$

$$Sh' = k_g D_p / D_v = \frac{3.65 \times 10^{-4}}{0.288} \times 17.8 = \underline{0.023.}$$

Then

$$Sh'_w = \frac{4\pi / \sqrt{3} \times 0.656}{\left[\frac{6 \times 0.216 \times 1 \times 3600}{0.434 \times (3.65 \times 10^{-4})^2 \times 336 \times 3.61}\right]^2} + 0.023 = \frac{k_w D_p}{D_v}$$

$$= 0.29 + 0.02 = 0.31.$$

ACKNOWLEDGEMENT

The stimulating discussions and overall assistance rendered by Professor William Brazelton of Northwestern University are greatly appreciated. Many thanks are extended to William Mecham and Albert Jonke of Argonne National Laboratory for their encouragement and to Professor Lowell B. Koppel, Research Associate at Argonne from Purdue University, for his vital work in the development of the heat transfer model.